https://doi.org/10.5194/egusphere-2026-1933
Preprint. Discussion started: 8 May 2026

The missing drifts: Widespread and systematic underestimation of heterogeneity in mountain snow density and SWE across scales

Elijah N. Boardman[1], Karen L. Boardman[2], Christopher A. Jones[3], Sean D. Shipman[3], John A. Whiting[3,4], Joseph W. Boardman[5,6], Adrian A. Harpold[3]

[1]Mountain Hydrology LLC, Reno, NV, 89503, USA
[2]Independent scholar, Dubois, WY, 82513, USA
[3]Department of Natural Resources and Environmental Science, University of Nevada, Reno, Reno, NV, 89557, USA
[4]Graduate Program of Hydrological Sciences, University of Nevada, Reno, Reno, NV, 89557, USA
[5]Analytical Imaging and Geophysics LLC, Boulder, CO, 80305, USA
[6]Airborne Snow Observatories, Inc., Boulder, CO, 80305, USA

Correspondence to: Elijah N. Boardman (eli.boardman@mountainhydrology.com)

Abstract. Near-real-time estimates of mountain snow water equivalent (SWE) are essential for streamflow forecasting and other applications, and snowpack heterogeneity controls summer water supply volumes, peak flow magnitudes, and other snowmelt runoff dynamics. Spatially resolved SWE quantification often depends on extrapolation from sparse regional measurements. When these measurements are not representative, the resulting spatial datasets are misleading. Here, we leverage complete density profiles from 36 snow pits (including eight at least 2 m deep) and repeat airborne lidar surveys spanning the Wind River Range (Wyoming, USA) to quantify missing heterogeneity in widely available snow density and SWE datasets at the point scale, grid scale (3 m to 1 km), and watershed scale. Our field measurements strategically constrain expected endmembers of snowpack variability, including rarely sampled snowpack zones such as deep drifts, steep slopes, avalanche runouts, and high elevations. Complete vertical profiling of a 5.9 m drift in a nivation hollow reveals a bulk density of 585 kg/m^3, rivaling the density of avalanche debris and exceeding the predictions of prior empirical snow density models by 14% to 35%. In contrast, we contemporaneously observe bulk densities as low as 339 kg/m^3 in adjacent forested areas. All 88 of the in-situ daily snow monitoring sites (SNOTEL) in the State of Wyoming are located in forested areas, which cannot account for alpine snowpack heterogeneity. This missing density and depth heterogeneity propagates into watershed-scale assessments. Across three large-domain near-real-time gridded SWE datasets, the standard deviation of SWE at the 500 m grid-scale is underestimated by 33% to 75% compared to our lidar-based data aggregated to the same resolution. These extrapolated SWE datasets underestimate the snowpack storage in a heavily drifted 1 km^2 glacial cirque basin by 65% to 73% despite only 2% to 17% underestimation of watershed-average SWE, underscoring the problem of missing heterogeneity. Spatially resolved SWE quantification in mountain regions can benefit from lidar and strategic field density sampling to better account for dense wind drifts and other drivers of heterogeneity in near-real-time.

https://doi.org/10.5194/egusphere-2026-1933
Preprint. Discussion started: 8 May 2026

1 Introduction

Mountain snowpacks are a global water resource (Mankin et al. 2015, Immerzeel et al. 2020), and quantifying seasonal snow water equivalent (SWE) is useful for predicting seasonal water supply availability (e.g., Pagano et al. 2004, Fleming et al. 2023), constraining the glaciological mass balance (e.g., Zemp et al. 2009, Dadic et al. 2010, Medley et al. 2013), and understanding mountain hydrology in general (e.g., Bales et al. 2006, Li et al. 2017). The spatial distribution of the snowpack provides a qualitatively different type of information beyond the basin-mean volume and is determined by physical processes interacting across a wide range of scales (Mott et al. 2010). Snowpack heterogeneity influences snowmelt runoff timing, peak flow magnitude, late-season runoff volumes, ecological processes, glacier dynamics, and more (Luce et al. 1998, Lundquist et al. 2005, Brauchli et al. 2017, Freudiger et al. 2017, Schneider et al. 2020, Marsh et al. 2024, Wigmore and Molotch 2024, Boardman et al. 2025, Pfohl et al. in review). Many methods have been proposed to quantify the spatial distribution of mountain snow water equivalent (SWE), broadly based on some combination of remote sensing, modeling, and extrapolation from ground-based measurements (Dozier et al. 2016, Yang et al. 2023, Mortimer et al. 2024). Although many novel techniques have been proposed for spatial SWE estimation, most datasets that are currently available across continental scales in near-real-time are based on combination of statistical extrapolation and data assimilation into physical models. Here, we test whether these widespread datasets and models capture the types of heterogeneity observed in field data from a heavily wind-affected alpine mountain region (Boardman et al. 2025). The contribution of snow density to overall snowpack heterogeneity remains particularly uncertain, since snow depth heterogeneity can be well-constrained through airborne lidar surveys (Painter et al. 2016).

Variability in snow depth and snow density both contribute to spatial heterogeneity in SWE. Field surveys and automatic monitoring stations can measure both of these properties, but measuring snow depth is comparatively easy, and density is expected to be less variable over space and time, so snow depth measurements have traditionally been much more abundant compared to density or SWE measurements (Elder et al. 1998, Erxleben et al. 2002, Sturm et al. 2010). In recent decades, the Airborne Snow Observatory (ASO) approach to lidar remote sensing (Painter et al. 2016) has further increased the discrepancy between abundant snow depth measurements and sparse density measurements (Raleigh and Small 2017, Broxton et al. 2019). Airborne lidar surveys can provide maps of snow depth across entire mountain ranges at resolutions of 1-3 m (Hopkinson et al. 2004, Deems et al. 2013, Painter et al. 2016). Converting these snow depth maps into SWE requires constraining spatiotemporal variability in snow density across complex terrain, which is the largest source of uncertainty in lidar-based SWE surveys (Raleigh and Small 2017). Snow density information is also useful for other remote sensing approaches to mapping SWE, including photogrammetry (e.g., Bühler et al. 2015, Nolan et al. 2015), some radar-based methods (e.g., Rutter et al. 2019, Tsang et al. 2022), and passive microwave methods (e.g., Venäläinen et al. 2021). Snow density may also be obtained from the combination of radar and lidar remote sensing in some conditions, i.e., in shallow dry snow (Meehan et al. 2024).

https://doi.org/10.5194/egusphere-2026-1933
Preprint. Discussion started: 8 May 2026

Several approaches have been developed to constrain snow density, including process-based modeling and data assimilation (e.g., Hedrick et al. 2018), empirical extrapolation from field measurements (e.g., Jonas et al. 2009), machine learning approaches (e.g., Sun et al. 2024), or simple mean aggregation from automatic monitoring stations (e.g., Kirchner et al. 2014). However, these methods are considerably uncertain due to the sparsity of observational density data, especially in alpine locations (Molotch and Bales 2006). Similar uncertainties arise in physical model-based approaches, as process-based snow models suffer from incomplete physics (Keenan et al. 2021) and uncertain forcing data (Raleigh et al. 2015). As a result, distributed model estimates of snow density are typically bias-corrected using the same sparse ground measurements (e.g., snow pillows and field surveys), so even these model-based density fields are ultimately influenced by extrapolation with respect to elevation-density trends, depth-density trends, and other density biases (Painter et al. 2016, and see also numerous ASO survey reports). Wind-snow interactions are particularly important for capturing the distribution and density of alpine snow drifts, but wind fields are notoriously challenging to model in complex terrain (e.g., Raderschall et al. 2008, Mott and Lehning 2010, Musselman et al. 2015). Data-driven empirical models of snow density are agnostic to uncertain process representations (Avanzi et al. 2015), but these correlations are often weak and inconsistent (López-Moreno et al. 2013, Wetlaufer et al. 2016). Moreover, in-situ and manual field measurements rarely constrain snow density in inaccessible locations such as high elevations, deep drifts, and steep slopes (Molotch and Bales 2006, Wirz et al. 2011, Grünewald et al. 2013), limiting our ability to test, improve, and validate model assumptions.

Spatial heterogeneity in snow density is the product of complex interactions between the atmosphere, the land surface, and the snowpack itself (Seligman 1936, Mellor 1964, Pomeroy et al. 1998). The evolution and spatial variability of snow density begins with the variable fresh snowfall density and unique depositional history of each location and year (Judson and Doesken 2000, Roebber et al. 2003). As the snowpack evolves, a wide array of processes contribute to density variations, including the settling and compaction of snow grains, the percolation and refreezing of liquid water, and the metamorphosis or diagenesis of snow grains into different shapes (Anderson and Benson 1963, Sommerfeld and LaChapelle 1970, Colbeck 1982, Brun 1989, Marshall et al. 1999). In forested locations, tree canopies mediate snowpack dynamics by intercepting and releasing precipitation, decreasing solar radiation, increasing thermal radiation, and reducing wind speeds (Rutter et al. 2009, Varhola et al. 2010, Safa et al. 2021). The local microclimates created by forest canopies can further modulate snow density relative to open locations (Pomeroy et al. 1998, Bonner et al. 2022).

In addition to spatial (lateral) variability, snow density varies vertically as a consequence of depositional history, thermodynamic gradients, and mechanical stresses within the snowpack (Colbeck 1991, Harper and Bradford 2003, Hao et al. 2021). Strong snowpack temperature gradients (i.e., cold atmospheric conditions) can cause the development of low-density snow layers with large faceted crystals, particularly near the ground, which is known as “depth hoar” (Seligman 1936, Akitaya 1974, Sturm and Benson 1997, Domine et al. 2018). Wind-blown snow is associated with the development of

https://doi.org/10.5194/egusphere-2026-1933
Preprint. Discussion started: 8 May 2026

high-density surface layers ("wind slab") due to the mechanical fracturing of snow grains during saltation and possibly other processes involving humidity feedbacks, a phenomenon known as "wind-packing" (Mellor 1964, Craven and Allison 1998, Fierz et al. 2009, Sommer et al. 2017). Finally, deep snow evolves into firn and ultimately ice over multiple years through a combination of densification processes caused by overburden pressure and thermodynamic gradients, including grain rearrangement (compaction) and recrystallization (Anderson and Benson 1963, Alley et al. 1982, Arnaud et al. 1998, Hörhold et al. 2011). Although the nuances of these processes have been considered in the observational literature for many decades, many of these processes are missing from the actual operational models used in near-real-time to estimate density fields in concert with airborne lidar snow depths. For example, the version of iSnobal used by Hedrick et al. (2018) to estimate SWE in combination with lidar data only considers temperature metamorphism, liquid water content, compaction from overburden pressure, and time since accumulation as a heuristic for unsimulated grain-scale processes. Thus, it is unknown to what degree the common practice of neglecting other controls on alpine snow density (wind-packing, avalanches, etc.) might impact near-real-time spatial snowpack assessments used for water supply forecasting.

The density of deep alpine snow is especially poorly constrained despite considerable glaciological and hydrological importance. In-situ measurements of snow density, e.g., SNOw TELemetry (SNOTEL) stations in the USA, are concentrated in forested regions within a relatively narrow elevation band, and these stations are not representative of the snowpack above treeline (Molotch and Bales 2006). Manual field surveys likewise tend to neglect inaccessible and potentially dangerous alpine regions, so complete snow pit profiles from deep drifts are rare in the literature. For example, one of the most comprehensive and well-funded snow surveys recently conducted in the western USA (Meehan et al. 2024) obtained 155 snow pit density profiles over many weeks, but their deepest snow pit was 1.43 m, considerably less than the threshold of 1.5 to 2 m SWE (3 to 4 m snow depth) that is important for glacier resilience and streamflow timing in alpine regions (Boardman et al. 2025). Deep wind-drifted snow and avalanche debris persists later into the summer compared to nearby shallower snow, so deep snow has outsized importance for mediating streamflow timing and sustaining perennial snow and ice below the regional equilibrium line altitude (Luce et al. 1998, Florentine et al. 2018, Mott et al. 2019, Boardman et al. 2025). Prior studies of deep snow density tend to focus on the evolution of glacial firn, where multiple years of snow compaction leads to higher densities farther below the surface. For example, firn measurements from an Alaskan glacier show spring snow densities below 400 kg/m^3 near the surface and exceeding 600 kg/m^3 at a depth of roughly 10 m (Stevens et al. 2024). Unlike glacial firn, which persists across multiple years by definition, kilometer-scale snow transport by wind and avalanches can yield seasonal accumulation of 4-6 m SWE (3-9 times local mean snowfall), even in locations that become snow-free every year (Boardman 2025). Over geological timescales, these deep snow drifts coevolve with the local topography in a process known as "nivation." The resultant "nivation hollows" are shallow topographic depressions caused by a positive feedback cycle between snow persistence and accelerated weathering: a deepening hollow causes a larger (and more persistent) snow drift by locally reducing the wind speed, and the persistent snow drift provides an enhanced source of meltwater that drives rock dissolution and other erosive processes (e.g., Henderson 1956, Thorn 1976, Dohrenwend 1984).

https://doi.org/10.5194/egusphere-2026-1933
Preprint. Discussion started: 8 May 2026

To our knowledge, complete vertical snow density profiles from deep (≥ 4 m) seasonal alpine wind drifts are not reported in the literature. Due to the logistical difficulty of digging and sampling very deep snow pits, vertical snow density profiles are typically only measured over the upper 1-2 m of the snowpack, even in areas where total snow depths may be much deeper (e.g., Schaerer 1988, Kanamori et al. 2005, Libois et al. 2014). It is thus an open question whether these shallower snow pits are sufficient to constrain alpine snow density at watershed scales. Tabler (1980) reports snow densities from deep artificial wind drifts (downwind of snow fences) measured using a Federal sampler (snow coring tube), which does not provide information on vertical density heterogeneity. Sturm et al. (2001) measured the density of wind slab strata in a deep Arctic drift, finding a much higher average density compared to nearby tundra snow (mean 398 vs. 300 kg/m^3), but they did not report complete ground-to-surface density profiles.

In the present study, we investigate snow density heterogeneity across an alpine mountain range by measuring complete vertical snow pit profiles in varied settings including deep drifts to address our first research question: To what extent does snow drift density contribute to alpine snowpack heterogeneity compared to other drivers of variability such as elevation, slope, and forest cover? We explore interactions between wind and snow density through two detailed site comparisons and numerical wind modeling at a deep drift location. Comparing our snow pit observations with prior empirical density models and regional SNOTEL data addresses our second research question: How well do existing datasets and regression models account for this observed density heterogeneity? After combining a new Bayesian regression density model with a lidar snow depth survey, we compare our estimated SWE map (delivered to managers and stakeholders in near-real-time) with other gridded SWE datasets to address our third research question: How well do widely available near-real-time spatial snowpack datasets account for snowpack heterogeneity across mountain watersheds?

2 Methods

The present study focuses on the results of snow surveys conducted in the Wind River Range (WRR), Wyoming, USA, from May 25 through June 2, 2025. This timeframe corresponds to the early ablation season in the WRR, and while the ephemeral low-elevation snowpack had already melted completely, portions of the high-elevation snowpack were not yet isothermal (snow temperature < 0 ˚C). Prior snowpack modeling, streamflow analysis, and extensive field experience suggests that most snowmelt occurs beginning in late May through July in alpine regions of the WRR (Boardman et al. 2025, Boardman 2025).

We begin by describing our field measurement protocols and survey design, and we subsequently analyze controls on snow depth and density using geospatial data and wind modeling. We then test several widely cited statistical snow density models to test whether they capture our measured axes of heterogeneity, and we compare our estimated SWE map with other near-real-time gridded SWE datasets across three watersheds (Fig. S1 in the Supplement).

https://doi.org/10.5194/egusphere-2026-1933
Preprint. Discussion started: 8 May 2026

All statistical hypothesis tests presented throughout are conducted using the Welch two-sample two-sided t-test or the Pearson product-moment correlation test as implemented in the R statistical programing language.

2.1 Field Measurements

The primary motivation for our WRR snow field surveys is to constrain spatial variability in snow density in order to estimate a spatial map of SWE from airborne lidar snow depth maps in support of water supply forecasting. Thus, our surveys are designed to sample hypothesized endmembers of variability: deep vs. shallow snow, low vs. high elevations, forested vs. open areas, different slope aspects, and unique types of snow such as avalanche debris. This is similar to the approach of Broxton et al. (2019), who also used snow pits to constrain anticipated endmembers of variability. Unlike many snow field surveys, we prioritize snow density instead of depth measurements since high resolution depth data are available from the airborne lidar surveys. Additionally, we only collect snow pit measurements instead of using a SWE coring tube (i.e., Federal sampler) because deep, high-density snow with icy layers is not conducive to inserting a sampling tube, and the rocky alpine ground is not conducive to obtaining a dirt plug to confirm that the ground was reached.

We conducted three fieldwork campaigns during the 2025 spring season. The first survey (May 24-26) involved six participants and yielded 13 snow pits, with a primary goal of digging and sampling one very large pit (5.9 m depth). We dedicated nearly a full day to digging this large pit and began measurements on the second day of the survey (May 25). The second survey (May 30-June 1) was conducted by a single individual and involved a traverse across the WRR to measure high-elevation snow on both sides of the mountain crest, yielding 18 snow pits. The third survey (June 1) involved two participants and yielded 5 snow pits. Combined, our three backcountry survey routes cover a distance of roughly 90 km with about 5,400 m of vertical elevation gain. Although we could sample more snow pits within a smaller area, traversing these substantial distances ensures that our measurements span a wide variety of representative terrain across the crest of the WRR (Fig. 1).

https://doi.org/10.5194/egusphere-2026-1933
Preprint. Discussion started: 8 May 2026

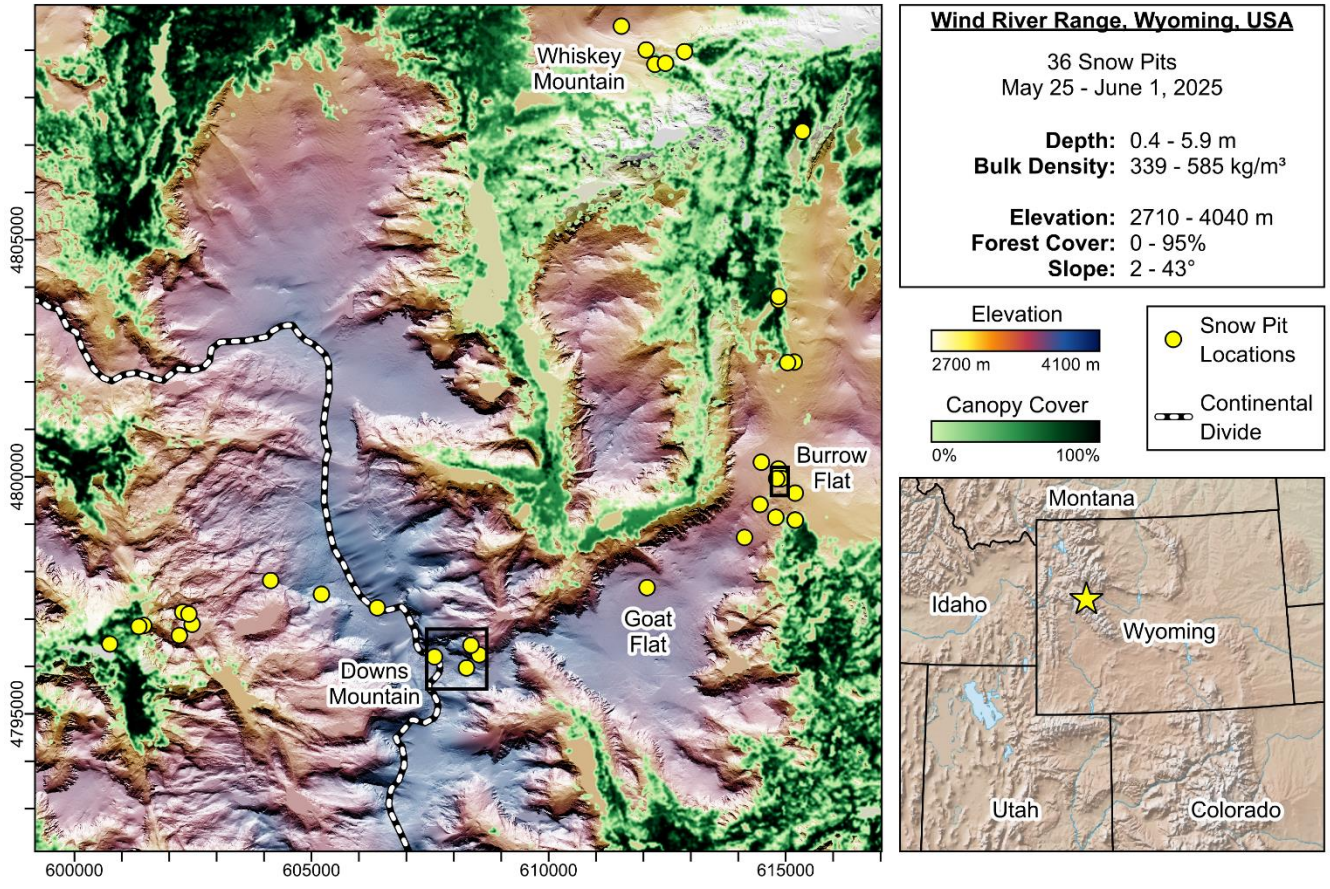

Figure 1. Overview map of snow pit locations and study site context within the Rocky Mountain region of the western United States.

At each snow pit, we measure vertical density profiles following standard protocols (Kinar and Pomeroy 2015). Most snow pits extend to the ground, identified by visual presence of rock/dirt. Two deep pits did not reach the ground due to time constraints, and we offset our height measurements for these pits using a combination of probe measurements and the 2025 lidar-based snow depths at the pit locations

We measure density using several 1,000 cc triangular wedge cutters (Snowmetrics Inc.), with care to ensure that the cutter is fully filled but not over-pressed into the snow face. To support a high level of precision, we re-tare the density cutter at each snow pit location to account for varying amounts of residual liquid water adhering to the cutter. Additionally, we carefully wipe off excess snow and liquid water from the outside of the cutter after each measurement, and we wipe out any snow adhering to the inside corners of the cutter before each new measurement. Despite our attention to detail, the precision of our density measurements is affected by the challenges of sampling dense, icy snowy in remote alpine locations, in addition to

https://doi.org/10.5194/egusphere-2026-1933
Preprint. Discussion started: 8 May 2026

the baseline uncertainty associated with all field density measurements (Proksch et al. 2016). In sections with density exceeding approximately 450 kg/m^3, we typically find it necessary to hammer in the density cutter using a dead blow mallet. Brittle, icy snow can chip out of the cutter, and in some cases it is necessary to replace these chips manually to approximate a full cutter sample. This "messy" quality of the data is inherent to the challenge of sampling vertical density profiles in extreme conditions, i.e., thick ice layers and brittle sub-zero snow in backcountry settings. All cutters remain visually free of deformation during our measurements. As a precaution, since hammering the cutter into hard snow could potentially degrade its precise geometry, we use a separate dedicated cutter for softer snow measurements. Calibration of both cutters by weighing the cutter when filled with liquid water indicates uncertainty of < 1% in the nominal cutter volume.

We also record supplemental data for each snow pit and measure snow temperature profiles using an analog thermometer. Calibration of the thermometer in ice water shows a nominal 0 ˚C. For each snow pit, we also take a variety of photos showing the regional setting and snow pit interior for archival reference and cross-checking with geospatial attributes such as forest cover. We record the location of each snow pit using a smartphone GPS, which has sufficient accuracy for our objective of estimating general geospatial attributes such as elevation and slope. Anecdotally, our deepest snow pit is clearly discernible in the airborne lidar data collected several days later, and our GPS point differs by less than one pixel (3 m).

2.2 Empirical Density Models

To explore potential drivers of spatial variability in alpine snow density, we construct a statistical regression model fine-tuned to our 2025 WRR dataset, and we compare our results with several generalized empirical models from the literature to test whether these other models predict similar degrees of variability.

2.2.1 Bayesian Density Modeling from Snow Pit Data

Based on several previous years of regional snow measurements from the WRR, in Boardman et al. (2025) we posited an empirical density model with three variables: snow depth, elevation, and forest cover. The elevation and forest cover terms are nonlinear to represent a potential ripening elevation (where the density changes fastest) and the threshold-like effect of thin forest cover. Here, we extend this model to include linear relationships with the north slope and east slope variables introduced in Sect. 2.2.1. The updated version of the model (Eq. 1) has nine parameters (θ1-θ9) and is sensitive to five variables (D = snow depth in m, E = elevation in km, C = fractional forest canopy cover, NS = north apparent slope in degrees, ES = east apparent slope in degrees).

$$\rho = \theta_1 + \theta_2 D + \frac{\theta_3}{1 + e^{-\theta_4 (E - \theta_5)}} + \theta_6 \left(1 - \frac{\theta_7}{C + \theta_7}\right) + \theta_8 NS + \theta_9 ES \quad (1)$$

Elevation is extracted from the lidar DTM. To capture hillslope-scale slope/aspect relationships instead of spurious slopes (e.g., associated with individual talus blocks), we aggregate the DTM to 30 m resolution before calculating slope and aspect.

https://doi.org/10.5194/egusphere-2026-1933
Preprint. Discussion started: 8 May 2026

Since aspect is discontinuous at 0-360˚, we combine slope and aspect into the commonly used "north slope" and "east slope" metrics, sometimes referred to as "northness" and "eastness," and defined as the apparent dip of the hillslope in the respective direction. Finally, we estimate forest canopy cover at each snow pit location. Our primary approach to forest cover is based on the RCMAP 30 m fractional tree cover dataset (Rigge et al. 2021), reprojected to 3 m using Lanczos spline interpolation. Like any gridded geospatial dataset, RCMAP exhibits erroneous values in some locations, so for some snow pits, we replace false zero values in RCMAP with estimates of canopy cover based on field observations and adjacent RCMAP pixels. Although the exact fractional forest cover value is uncertain for any single snow pit due to the nature of extracting point values from raster data, the categorization as "forested" or "open" is well-constrained by field observations.

A Bayesian statistical framework provides estimates of the Eq. 1 parameters while simultaneously quantifying the uncertainty of the model. We sample Eq. 1 assuming a normal distribution of snow density errors with individual measurements weighted based on their "representativeness" compared to the entire lidar-surveyed snowpack, as described by Boardman et al. (2025). Since this approach to weighted Bayesian model-fitting is key to the statistical robustness of our resulting gridded density field, we review the method in greater detail here, though it is essentially unchanged from the previous description and implementation by Boardman et al. (2025). The representativeness score is intended to approximate the degree to which each snow pit is the best match for bulk SWE at the watershed scale, i.e., the most representative snow pits that those are similar to relatively large areas and/or relatively deep areas of the lidar-surveyed snowpack, since these large and/or deep areas store relatively more SWE (by definition).

Algorithm: Calculate Density Representativeness

(1) Linearly re-scale predictor variables relative to valid range (0 to 6 m snow depth, 2500 to 4200 m elevation, 0% to 100% canopy cover, -90° to 90° north and east slope).
(2) Randomly sample 10^6 pixels from the lidar snow depth map with sampling probability proportional to snow depth, since deeper areas hold more SWE per unit area and are thus more important on a pixel-wise basis. For example, a single 2 m pixel is twice as likely to be sampled as a single 1 m pixel, but if there are twice as many 1 m pixels present on the landscape, both depth ranges would be sampled equally.
(3) For each snow depth pixel sample:
    (a) Calculate the Euclidean distance between the re-scaled predictors at that pixel location and the re-scaled predictors for each snow pit.
    (b) Identify the snow pit that is closest (in predictor-space) to the pixel sample, and increment that snow pit's "number of explained pixels" by one.
(4) The representativeness of each snow pit is defined by its number of explained pixels divided by the 10^6 sample size, plus one percent (so that each snow pit is guaranteed to be included in the model).

https://doi.org/10.5194/egusphere-2026-1933
Preprint. Discussion started: 8 May 2026

The above-defined snow pit representativeness score is used to implement a statistically rigorous weighted model-fitting procedure. Specifically, we perform weighted log-likelihood Bayesian sampling of the parameters in Eq. 1 using Hamiltonian Monte Carlo (HMC) implemented in Stan (Stan Development Team 2023). The representativeness score is multiplied by the log likelihood of each snow pit observation, which pushes the model to more closely match snow pits that are particularly representative (Eq. 2).

$$P(\theta \mid y, r) \propto P(\theta) \prod_{i=1}^{N} \mathcal{N}(y_i \mid \mu_i, \sigma)^{r_i} \quad (2)$$

In Eq. 2, the posterior parameter distribution (left side of equation) is proportional to the prior parameter distribution and the product of the normal probability density function raised to the power of the weights, with N datapoints, y indicating observations (snow pit densities), μ indicating the model mean, σ indicating model standard error, and r indicating the likelihood weights (representativeness score). Note that the weights are exponentiated in Eq. 2 because they are multiplicative with respect to the log-likelihood (the model optimization target). Prior parameter distributions (Fig. S2 in the Supplement) are mildly informative to initialize the model into a physically plausible domain based on prior modeling in the WRR (Boardman et al. 2025), but the posterior distributions are substantially transformed, reflecting the impact of the data (Fig. S3 in the Supplement).

The HMC Bayesian sampler receives 10,000 warmup iterations and generates 1,000 final samples. Effective sample sizes and sample plots are consistent with convergence. We evaluate Eq. 1 using all 1,000 parameter samples, thereby generating a Bayesian posterior distribution for snow density at each pixel, and we calculate the mean predicted density of each pixel to estimate SWE. We also evaluate the previous iteration of our snow density model (no NS or ES dependence) using the previously sampled 2024 parameter values (Boardman et al. 2025) to test whether snow density patterns repeat across years.

2.2.2 Comparison with Previous Literature Models

Next, we test several other empirical snow density models described in the literature, introduced here in chronological order (Table 1). Tabler (2003) models snow density based solely on a nonlinear function of snow depth, with parameter values based on measurements from artificial drifts created by snow fences in Wyoming. Jonas et al. (2009) similarly use monthly lookup tables to model density as a linear function of depth in the Swiss Alps. Since our measurements span the end of May and the first day of June, we average the Jonas et al. (2009) parameters from both months. Sturm et al. (2010) model density as a nonlinear function of depth and day of year, with parameter values based on snow climate class; Sturm et al. (1995) show that the WRR falls within the alpine climate class (Fig. 10 of that study). Bormann et al. (2013) model density using multiple linear regressions based on climatological metrics, with different combinations of variables selected for different regional classes. We evaluate two versions of the Bormann et al. (2013) model: one based on alpine sites from the USA, and one based on all sites across Australia, the USA, and the former USSR. Hill et al. (2019) model density as an exponential

https://doi.org/10.5194/egusphere-2026-1933
Preprint. Discussion started: 8 May 2026

function of depth, winter precipitation, the temperature difference between warmest and coldest months, and the day of water year.

Density Model	Equation
WRR 2025 Model (Eq. 1 of this study)	$\rho = 584 + 22\,D - \frac{317}{1 + e^{-1.5(E-3.47)}} - 144\left(1 - \frac{0.26}{C + 0.26}\right) - 39\,NS - 36\,ES$
WRR 2024 Model (Boardman et al. 2024)	$\rho = 568 + 15\,D - \frac{222}{1 + e^{-6.3\,(E-3.32)}} - 144\left(1 - \frac{0.06}{C + 0.06}\right)$
Tabler 2003	$\rho = 522 - \frac{304}{1.485\,D}(1 - e^{-1.485\,D})$
Jonas et al. 2009	$\rho = 14.5\,D + 415$
Sturm et al. 2010	$\rho = 373.8\,(1 - e^{-0.12\,D\,-0.0038\,DOY}) + 223.7$
Bormann et al. 2013 (Alpine Sites)	$\rho = \left(596 + 31.96\ln P1 - 3.56\,T_{avg}\ln D + 0.0392\,CDD - 3.94\,\lvert Lat\rvert - 29.98\,E\right) + 1.07\,(DOY - 60)$
Bormann et al. 2013 (Combined Sites)	$\rho = (566 + 47.95\,MRF + 32.67\ln P1 + 22.44\,\ln D - 3.82\,\lvert Lat\rvert - 29.95\,E) + 1.07\,(DOY - 60)$
Hill et al. 2019 (Ablation Season)	$\rho = \frac{1}{D}\,0.0481\,(D^{1.0395})\,(P2^{0.1699})\,(T_{diff}^{-0.0461})\,(DOWY^{0.1804})$

Table 1. Summary of empirical density models tested in this study. The snow density, ρ, is in units of kg/m^3. D = snow depth in m, E = elevation in km, C = fractional forest canopy cover, NS = north apparent slope in degrees, ES = east apparent slope in degrees, DOY = Julian day of year, DOWY = day of water year, P1 = December-March precipitation in cm/day, P2 = December-February precipitation in mm (1991-2020 climate normal), Tavg = December-March mean temperature in °C, Tdiff = mean temperature difference between warmest and coldest months in °C (1991-2020 climate normal), CDD = sum of daily mean temperatures below 0 °C during December-March, Lat = latitude in degrees, MRF = fraction of days with maximum temperature >0 °C and minimum temperature <0 °C during local snow cover season. Note that the WRR 2024 and WRR 2025 models are shown with median parameter values, but in practice, the density is predicted as an average across many Bayesian parameter samples. Equations are rearranged from their original form for readability and unit consistency.

The climatological models proposed by Bormann et al. (2013) require some adjustment for application to our field data, since these models were developed using continuous time series at long-term monitoring sites. We replace the maximum snow depth metric with the instantaneous snow depth at the time of our surveys. All climatological metrics are calculated from daily gridMET data (Abatzoglou 2013) after interpolating the meteorological data from approximately 4 km resolution to 90 m resolution using Lanczos spline interpolation. As specified by Bormann et al. (2013), most climatological metrics are averaged across December-March of the accumulation season prior to our measurements, with the exception of the melt-refreeze metric, which is calculated for a site-specific snow cover season. Based on field observations, the snow cover season is assumed to be November-June for the WRR. The Bormann et al. (2013) models predict snow depth on March 1, after which snow is assumed to densify at a constant rate. We apply the mean densification rate calculated by Bormann et al. (2013) for the USA alpine sites (1.07 kg/m^3 per day) over the period from March 1 to the date of each snow pit measurement. Since the Hill et al. (2019) model is explicitly intended for use with multi-year climate normals from gridded data instead of weather data from a particular year, we evaluate this model directly using the 1991-2020 gridMET normals reprojected as above.

https://doi.org/10.5194/egusphere-2026-1933
Preprint. Discussion started: 8 May 2026

To test the sensitivity of landscape-scale snowpack quantification to density model assumptions, we also apply each of these density models to the entire northern WRR snowpack at the time of the June 1-2, 2025, airborne lidar surveys. The climatological inputs are calculated at 30 m resolution for computation efficiency and resampled to the 3 m lidar snow depth resolution to estimate density. Congruent with our processing workflow for the dedicated WRR density model, all snow densities are limited to a plausible range of 300-600 kg/m^3.

2.3 Lidar-Based Snow Depth and SWE Data

Repeat airborne lidar surveys provide high resolution topography and snow depth data that inform our analysis of alpine snow variability. The snow-free topography of the WRR is captured by lidar acquired on August 18-19, 2019, distributed as a digital terrain model (DTM) by the U.S. Geological Survey (USGS) as part of the 3DEP program. Since glaciers and perennial snow/ice features are rapidly melting in the WRR, the snow-free DTM changes continually in many areas of the northern WRR. To account for annual ablation, we update the snow-free DTM using a dedicated glacier lidar survey conducted by Airborne Snow Observatories, Inc. (ASO) on October 7, 2024. Another lidar survey conducted by ASO on June 1-2, 2024, provides snow depth data at 3 m resolution across much of the WRR, including the full extent of our field surveys. Lidar processing procedures used for this project are presented in Painter et al. (2016) and Boardman et al. (2025). Our final SWE map (using ASO lidar depths with densities estimated from Eq. 1) was delivered to water managers and stakeholders on June 7, five days after the conclusion of the airborne surveys and two days after ASO's delivery of the snow depth map.

2.4 Comparison with Other SWE Datasets

Finally, we compare several other near-real-time gridded SWE datasets with our lidar-based dataset. Snow datasets selected for this comparison must be available in near-real-time, i.e., with a latency of days, since we are primarily interested in SWE quantification for water supply forecasting and related purposes. Additionally, we disregard very coarse datasets (larger than roughly 1 km resolution) that are unlikely to capture the relevant sub-watershed scales in the WRR region. We identify three qualifying datasets for this comparison: the SNOw Data Assimilation System (SNODAS) daily SWE product distributed by the National Oceanic and Atmospheric Administration (Barrett 2003), a regression-based SWE product (CU-SWE) distributed by the University of Colorado (Yang et al. 2022), and a neural network-based SWE product (SWANN) distributed by the University of Arizona (Broxton et al. 2016, 2019, 2024). For consistency and clarity, we refer to the two university experimental SWE products by their respective university names, i.e., U. Colorado SWE and U. Arizona SWE. The native resolutions of these products vary between 500 m for the U. Colorado dataset and 1/120° (approximately 800-1,000 m) for SNODAS and the U. Arizona dataset. For each of these products, in addition to the lidar-based SWE maps, we interpolate missing grid cell values using the average within a 3x3 kernel and reproject to a common 500 m resolution using the weighted average of overlapping cells. Using both the native resolution and the 500 m resolution, we calculate and

https://doi.org/10.5194/egusphere-2026-1933
Preprint. Discussion started: 8 May 2026

compare cumulative distribution functions (CDF) for SWE within each of three watershed boundaries encompassing our field survey area.

2.5 Wind-Topography Modeling

We also use the ASO snow-on and snow-off lidar topography data to explore the relationship between spatial snowpack heterogeneity and wind speed to test the hypothesis that wind-topography interactions can explain observed snowpack heterogeneity in our deepest sampled location. Slower wind speeds in sheltered locations can contribute to snow deposition and deep drift formation, which may also impact density due to wind-packing. We simulate wind speed for a 2.2 km^2 domain surrounding a major drift where our deepest snow pit is located. The WindNinja software (Wagenbrenner et al. 2019) leverages a computational fluid dynamics module based on a Reynolds-Average-Navier-Stokes (RANS) solver implemented in OpenFOAM (Weller et al. 1998). We use WindNinja to implement a RANS simulation of the wind field through a 3 m mesh restructured from the 1 m lidar DTM. We initialize WindNinja with a single 20 m/s west-to-east wind speed at a height of 10 m with a ground roughness length of 0.1 m (grass setting), and we sample the simulated wind field at 1 m height after 1,000 RANS solver iterations. Since our goal is merely to obtain an indicative map of faster/slower wind speeds, the precise numeric values are less important than the spatial pattern. This combination of settings proves satisfactory for illustrating the general slowdown and speedup of wind in the simulation domain, though it is merely a snapshot of hypothetical conditions and does not account for variability and uncertainty in the actual wind speed and direction. Secondly, we repeat this simulation with an altered DTM representing the snow surface, calculated by adding the 2025 ASO lidar snow depth to the 2019 snow-off topography.

3 Results

Our 2025 field surveys yield snow density data from 36 snow pits, 20 of which are at least 1 m deep and six of which are at least 2 m deep, with one 4 m pit and one 5.9 m pit. This volume of snow pit data is considerably larger than typically used for estimation of spatial density fields in lidar-based SWE mapping applications: for example, Kirchner et al. (2014) averaged snow density from 16 stations, Broxton et al. (2019) measured 17 snow pits (plus additional transects using a SWE coring tube), and Trujillo et al. (2025) relied on a snow density model with validation metrics from 11 sites in disparate mountain ranges. Other snow lidar surveys in the Wind River Range have relied on modeled densities with as few as two in-situ measurements used for bias-correction and validation (ASO Green River report for Upper Colorado River Commission survey on May 30, 2025). Some lidar-based snow surveys have used as many as 155 snow pits, but these data were collected across several weeks and the resulting spatial SWE data were not available in near-real-time (Meehan et al. 2024). Most prior snow surveys in the western USA rarely measure snow pits deeper than 2 m; for example, the deepest pit measured by Broxton et al. (2019) is 1.18 m, and only two of their pits are deeper than 1 m. Similarly, the dataset of 155 snow pits from Meehan et al. (2024) has a maximum measured depth of 1.43 m. Our study thus provides a unique opportunity to test the

https://doi.org/10.5194/egusphere-2026-1933
Preprint. Discussion started: 8 May 2026

hypothesis that underrepresentation of deep snow in prior surveys may lead to systematic biases when these data are extrapolated to windy alpine regions.

We first summarize the variability of measured snow density across the WRR (Fig. 1), including the spatial heterogeneity between locations and the vertical profiles within individual snow pits. We then analyze two locations in greater detail: a remarkably dense drift occupying a nivation hollow, and a high-elevation region illustrating a variety of interacting controls on density. Finally, we compare our measurements to empirical model predictions and gridded SWE datasets.

3.1 Snow Density Variability

Our measurements reveal substantial variability in ablation-season alpine snow density, both spatially and within individual pits (Fig. 2). The coefficient of variation (CV) among all 36 pits is 13% relative to a mean of 450 kg/m^3. The mean vertically integrated density (entire snow pits) varies between 339 and 585 kg/m^3, and individual density measurements (within pits) vary between 247 and 688 kg/m^3. The snow in forested areas is significantly ($p < 0.001$) less dense compared to snow in open areas (mean 405 vs. 471 kg/m^3). There is a significant correlation between snow depth and density ($r = 0.59$, $p < 0.001$), and snow at least 2 m deep is significantly ($p = 0.02$) more dense than snow that is less than 2 m deep (mean 497 vs. 438 kg/m^3). Additionally, snow at higher elevations is generally less dense. Although there is no significant correlation directly between elevation and density due to confounding variability, snow above 3500 m is significantly less dense ($p < 0.01$) than snow below 3500 m considering only non-forested locations (437 vs. 490 kg/m^3). However, we emphasize that these relationships are subject to multicollinearity, which prevents any straightforward interpretation. For example, there are significant correlations between elevation and forest cover ($r = -0.63$, $p < 0.001$) and between snow depth and forest cover ($r = -0.41$, $p = 0.01$) simply due to the existence of a treeline elevation and the lack of deep snow (> 2 m) in forested areas.

https://doi.org/10.5194/egusphere-2026-1933
Preprint. Discussion started: 8 May 2026

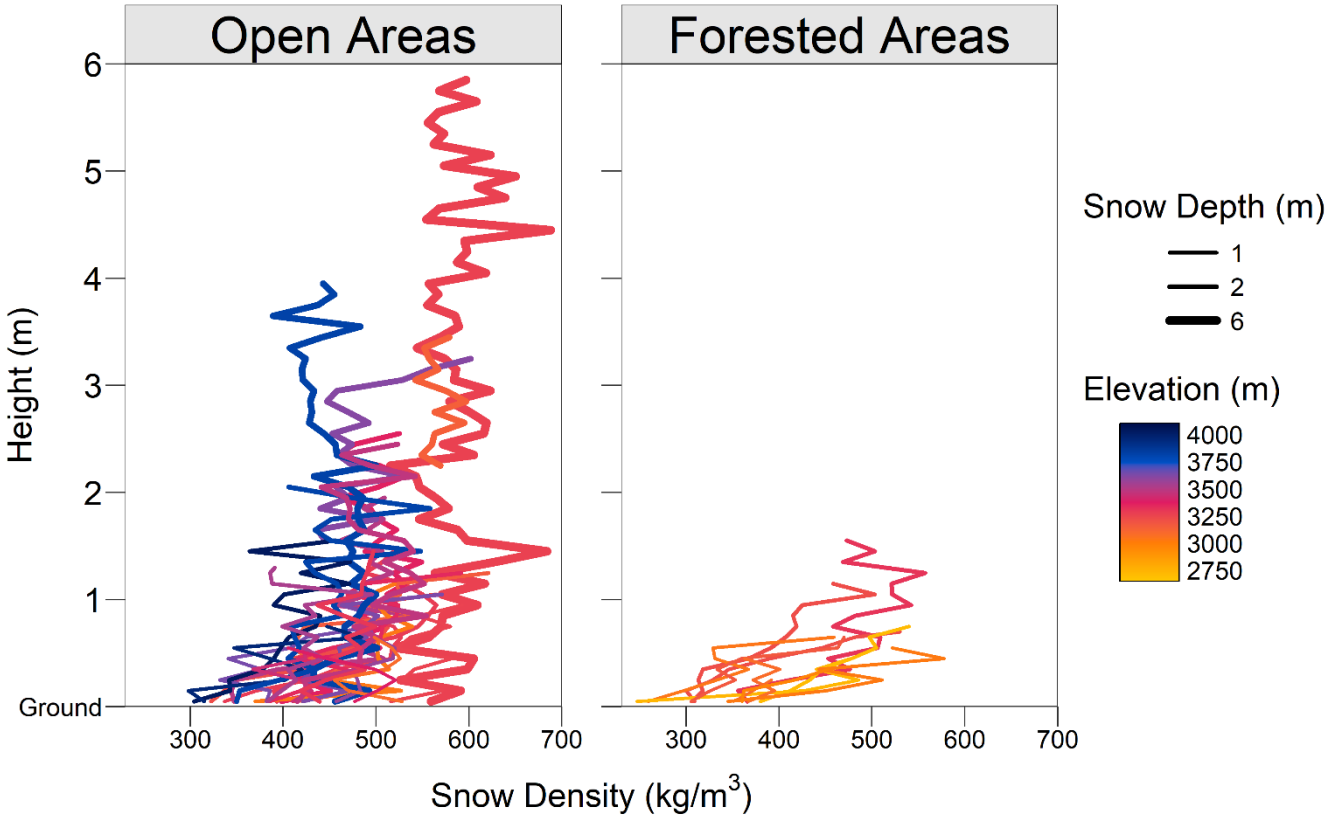

Figure 2. Vertical density profiles from 36 snow pits (locations in Fig. 1). The sampling resolution is 10 cm vertically. Note the non-representativeness of forested areas with respect to both snow depth and density.

There is less vertical variability in snow density compared to the spatial variability between pits, but vertical variability is still substantial. The standard deviation across all 485 individual density measurements is 75 kg/m^3, which reduces to 46 kg/m^3 after subtracting the mean of each snow pit from the constituent intra-pit measurements. For comparison, the standard deviation of mean density across all 36 pits is 57 kg/m^3, which is 22% more variable than the intra-pit vertical variability. Nevertheless, vertical trends in snow density can reveal salient information about physical processes operating in the snowpack that are missed by vertically integrated average measurements (such as those obtained from snow pillows or SWE coring tubes).

Isolating patterns of vertical density variability reveals several distinct categories of depth-density trends (Fig. 3). Most of the snow pits in forested areas have significant ($p < 0.05$) trends toward lower density near the ground (N = 8, or 73% of forested locations), and the other three have insignificant trends. Two of the three forested snow pits with insignificant depth-density trends nevertheless have lower-density snow near the ground, but the 10 cm vertical sampling resolution is too

https://doi.org/10.5194/egusphere-2026-1933
Preprint. Discussion started: 8 May 2026

sparse for the trend to rise to statistical significance in shallow snow. Among the 25 snow pits in open areas (non-forested), 13 have significant trends toward lower density near the ground and 11 have no significant trend. Interestingly, the snow pits with significant trends toward lower density near the ground have widely varying snow depths, from 0.4 m to 3.3 m. From field observations, we note that lower snow densities near the ground are commonly associated with depth hoar, i.e., faceted crystals caused by vapor gradients in shallow snow, though similar trends also emerge in deeper snow due to overlying avalanche debris and potentially other controls on densification.

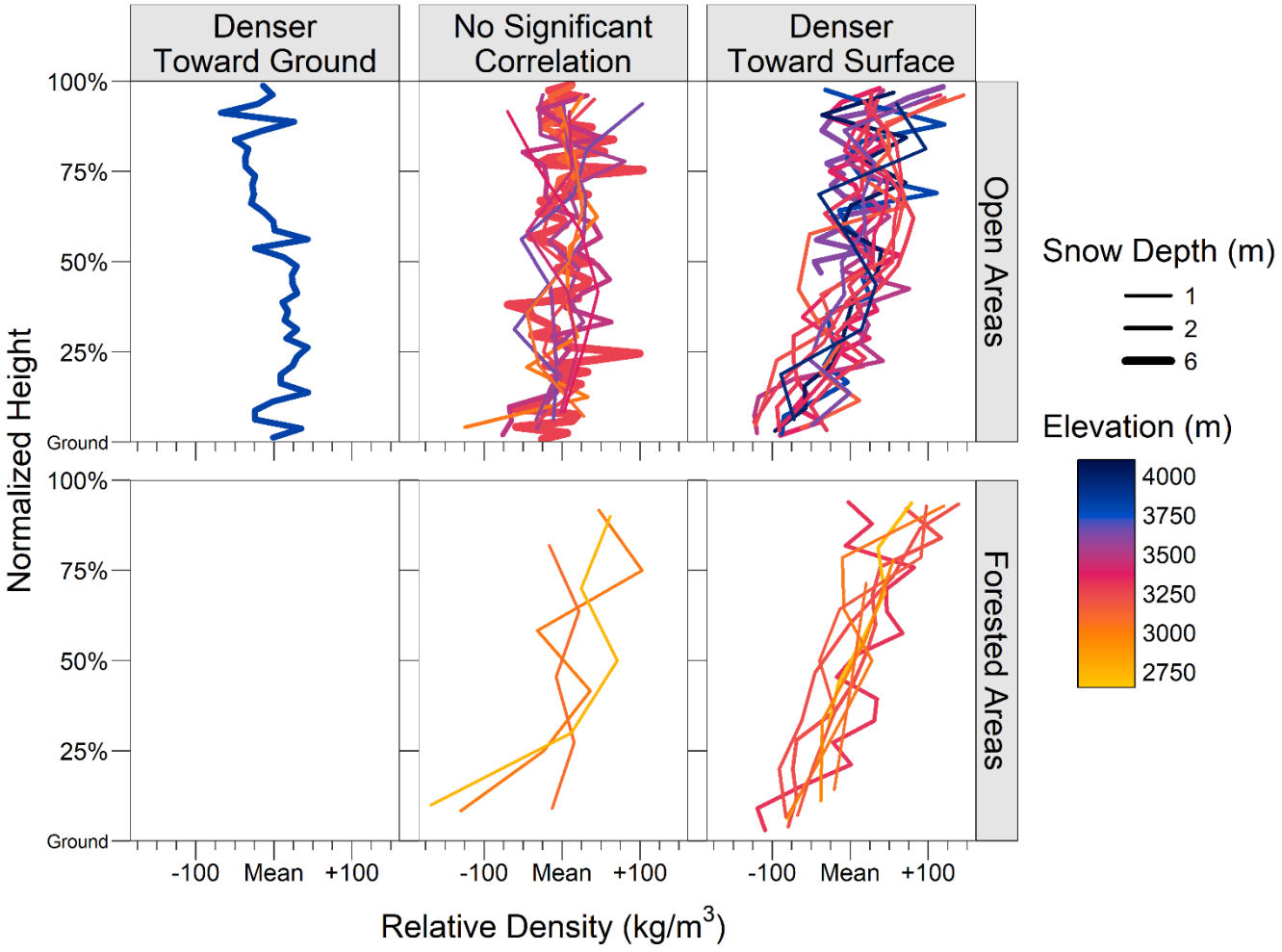

Figure 3. Vertical density trends relative to the mean density of each snow pit. Most snow pits have trends toward denser snow near the surface or no trend, and only one location has a trend toward denser snow near the ground. The threshold for trend significance is $p < 0.05$ using Pearson's product-moment correlation test.

https://doi.org/10.5194/egusphere-2026-1933
Preprint. Discussion started: 8 May 2026

Deep wind drifts exhibit different depth-density relationships compared to shallower snow. The deepest snow pit (5.9 m) has no significant trend with depth, a finding that we explore further in Sect. 3.2. The second-deepest (4.0 m) snow pit provides the sole example of a significant trend toward increasing density closer to the ground ($r = -0.53$, $p < 0.001$). Notably, this deep pit is at a relatively high elevation (3820 m) and had a mean temperature below freezing, which we explore further in Sect. 3.3. Thus, the lower density near the surface at this location could be associated with relatively fresh snow that has not undergone as much metamorphosis as the deeper, older snow.

3.2 Deep Drift Profile: Nivation Hollow

Measuring the density of a very deep snow drift was a key goal of our 2025 field surveys, since these deep drifts are salient features of the WRR landscape (Boardman et al. 2025, Boardman 2025). In this section, we focus our analysis on a wind drift occupying a nivation hollow at roughly 3280 m elevation near Burrow Flat in the Dinwoody Creek watershed (Fig. 1). Figure 4 provides an overview of our nivation hollow study site, including photographs of the drift surface and the interior of our deepest snow pit. A longitudinal profile across the nivation hollow shows how a nearly planar snow surface overlies a topographic concavity, which results in exceptionally deep snow near the middle of the drift (4-6 m).

https://doi.org/10.5194/egusphere-2026-1933
Preprint. Discussion started: 8 May 2026

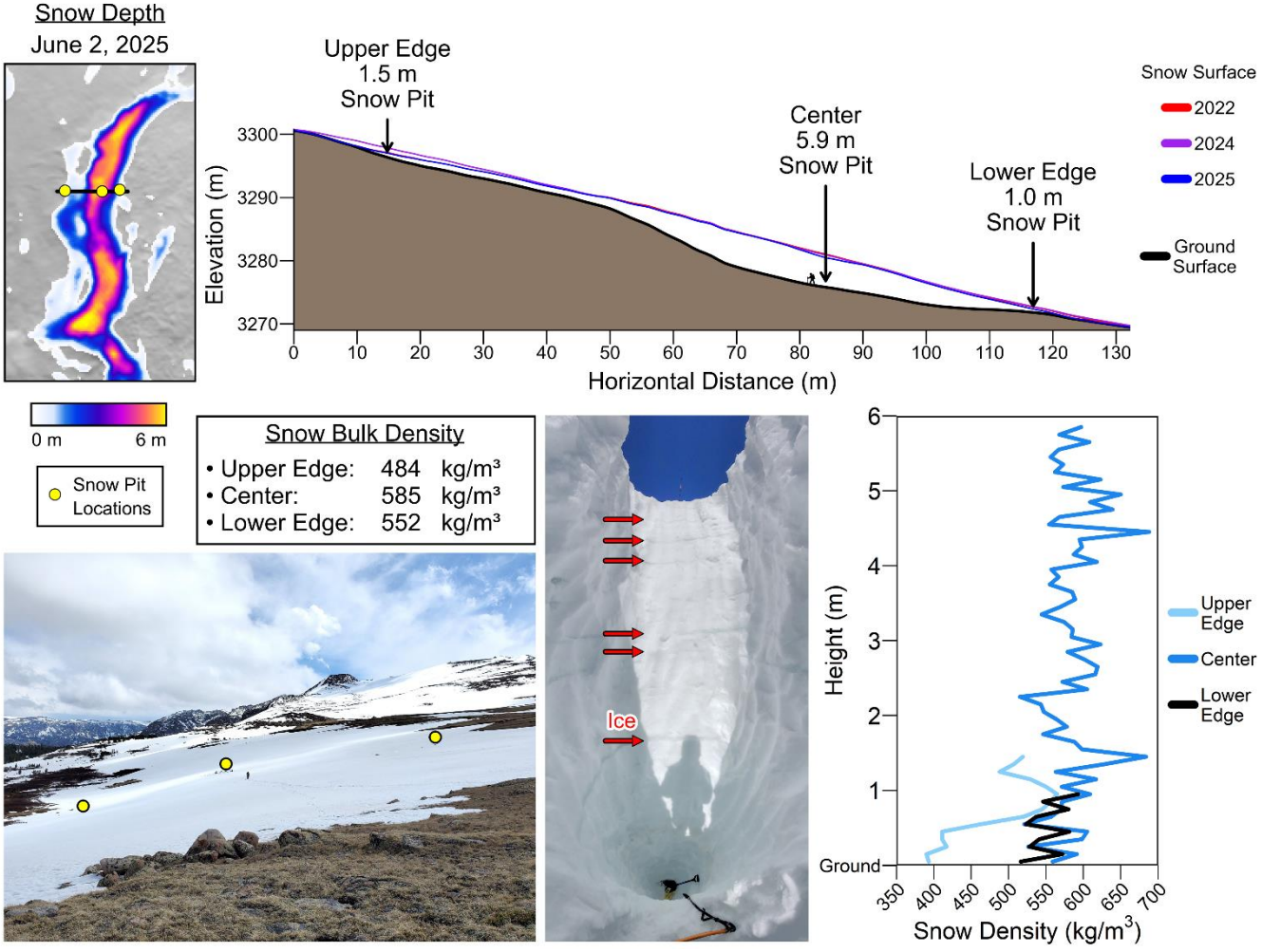

Figure 4. Snow depth profiles (longitudinal) and snow density profiles (vertical) from the Burrow Flat nivation hollow. Note that the longitudinal profile has the same horizontal and vertical scales. The human figure near the center snow pit arrow (in the depth profile) has an approximate height of 1.8 m (6 feet), and human figures are also visible in the overview photograph near the center snow pit. Major ice layers are indicated in the closeup photograph with red arrows, but there are also many thin ice layers near the surface that are not indicated.

A 5.9 m deep pit near the center of the nivation hollow reveals a remarkably high snow density, with a range of 515-688 kg/m^3 and a mean of 585 kg/m^3. There is no significant trend in density with depth for this deep pit ($r = 0.15$, $p = 0.24$). Nevertheless, the upper 2 m of the profile has a slightly higher density compared to the lowest 2 m of the profile (mean 595 vs. 582 kg/m^3), though this difference is not statistically significant. The deep drift remains quite dense even near the surface: the top meter has a mean density of 588 kg/m^3, and the top 10 cm has a density of 597 kg/m^3, both of which are higher than the pit average. These measurements support our qualitative observation that it is quite easy to walk on the surface of the nivation hollow drift without sinking in or "postholing," in contrast to nearby shallower snow.

https://doi.org/10.5194/egusphere-2026-1933
Preprint. Discussion started: 8 May 2026

We note several substantial ice layers (1-3 cm thick) beginning at a height of 2.2 m above the ground in the Burrow Flat nivation hollow drift. No horizontal ice layers are apparent below this height. Ice layers are more frequent closer to the surface, which may contribute to the higher bulk density of the upper 2 m of the pit. Notwithstanding, we still observe exceptionally high densities in deeper layers with no visible ice (e.g., 605, 628, and 684 kg/m^3 at 0.4-0.5, 1.3-1.4, and 1.4-1.5 m heights, respectively). A re-frozen preferential "flow finger" (Marsh and Woo 1984) was encountered at approximately 1.0-1.4 m height, but we chose to avoid sampling this anomalous feature and instead sampled adjacent snow without visible ice. Surprisingly, our lowest-density measurement (515 kg/m^3 at 2.2-2.3 m height) is associated with the deepest and thickest ice layer (approximately 3 cm thick). Our highest-density measurement (688 kg/m^3 at 4.4-4.5 m height) is also associated with several thinner ice layers. One explanation for this discrepancy could be different amounts of liquid water pooling/refreezing above and below the different ice layers, especially if the ice layers create preferential lateral flow pathways. However, these ice-layer measurements are also relatively uncertain due to the inherent challenge of sampling brittle ice with a metal density cutter, and the anomalous weights could be the result of measurement error.

Additional snow pit measurements reveal that density remains unexpectedly high near the lower edge of the nivation hollow, but snow at the upper edge is more comparable to the density of nearby locations. Based on prior fieldwork, we anticipated that shallower snow (< 2 m) would have a lower density more in line with the 350-450 kg/m^3 range of typical ablation-season alpine snow. While this is largely true at the landscape scale (Fig. 2), a 1.0 m snow pit near the lower edge of the nivation hollow has a mean density of 552 kg/m^3, only 6% lower density than the deep pit near the middle of the drift. Interestingly, the 10 samples from this shallower snow pit have a high correlation with the lowest 10 samples from the deep pit ($r = 0.76$, $p = 0.01$), indicating that both locations have similar density stratigraphy near the ground. This increases our confidence that vertical density variations are physically meaningful (not just the result of random sampling error), and seemingly implies that the processes controlling densification are independent of snow depth within parts of the nivation hollow drift. In contrast, a 1.5 m snow pit near the upper edge of the nivation hollow shows a different signature: its mean density of 484 kg/m^3 is 17% lower than the center of the drift, and there is no significant correlation between the vertical density variation of the 1.5 m pit and the bottom 1.5 m of the deep pit ($r = 0.23$, $p = 0.41$). The upper edge of the nivation hollow drift fits within the density range of surrounding snow (mean density range 444-488 kg/m^3 across five other pits in non-forested locations).

Wind simulations and repeat lidar observations indicate that the nivation hollow reduces wind speed until it fills with snow, resulting in an apparent self-limiting drift behavior (Fig. 5). The mid-July imagery in Fig. 5A shows how the deep drift persists through much of the summer after most other snow has melted, though field observations indicate that it melts out completely by September, at least in most years. Simulating the wind speed 1 m above the underlying ground surface results in a wind speed pattern that closely mirrors the snow depth pattern (Fig. 5B, D-F). Wind speeds are greatly reduced where

https://doi.org/10.5194/egusphere-2026-1933
Preprint. Discussion started: 8 May 2026

the concave nivation hollow creates a sheltered zone, similar to the functioning of artificial snow fences. Snow transport is reduced in areas with lower wind speeds, which reduces the suspension and saltation fluxes, causing drift formation. Consequentially, we there is a strong negative correlation between ground wind speed and snow depth ($r = -0.71$, $p < 0.001$). However, as the nivation hollow begins to fill with drifted snow, the topographic concavity has less effect on the wind speed. The wind speed 1 m above the 2025 snow surface is much faster than the wind speed 1 m above the ground surface (Fig. 5C). In areas with > 4 m snow depth, the mean wind speed is 143% faster above the snow surface compared to the ground surface.

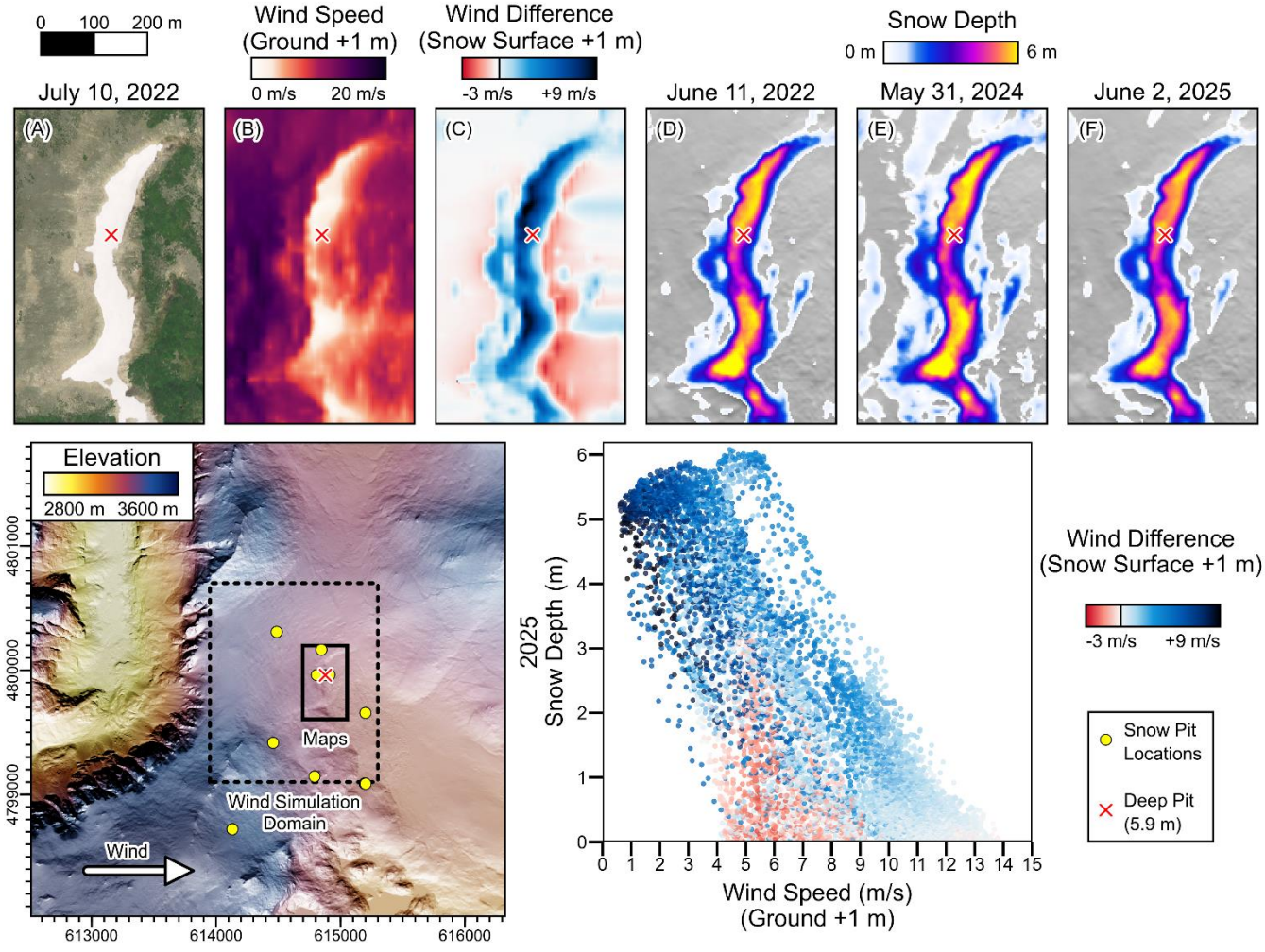

Figure 5. Wind speed simulations and annual snow depth maps associated with the Burrow Flat nivation hollow.

https://doi.org/10.5194/egusphere-2026-1933
Preprint. Discussion started: 8 May 2026

The nivation hollow wind drift stores nearly the same amount of snow each spring (Figs. 4-5) despite widely varying seasonal snowfall. For example, based on spatially complete lidar depth data with densities constrained by our fieldwork, we estimate that the surrounding Dinwoody Creek watershed has a mean snowpack storage of 0.21 m SWE on June 2, 2025, compared to 0.34 m on May 31, 2024, which is 37% less in 2025 at nearly the same point in the season. However, areas of the nivation hollow with > 4 m snow depth in 2025 (0.015 km^2 area) had a mean snow depth decrease of 0.36 m relative to 2024, representing an estimated SWE volume storage difference of only 7% in those locations. As illustrated in the Fig. 4 profile and the Fig. 5 maps, nearly identical snow surface elevations are observed by three different airborne lidar surveys: June 11, 2022; May 31, 2024; and June 1-2, 2025. The snow depth correlations between all three lidar survey pairs range between $r = 0.98$ and $r = 0.99$ ($p < 0.001$) in the drift vicinity at the 3 m grid scale (Fig. 5D-F).

Another nivation hollow at a similar elevation of 3140 m on nearby Whiskey Mountain (Fig. 1) exhibits a similarly high bulk snow density. A partial snow pit in this nivation hollow drift (top 1.3 m sampled of 3.5 m total depth) has a mean density of 567 kg/m^3, again with no significant depth-density trend ($r = -0.02$). This represents the second-highest mean snow density recorded during our 2025 field surveys, and all three snow pits with mean densities above 500 kg/m^3 are associated with wind drifts in nivation hollows (Burrow Flat drift center, Whiskey Mountain drift, Burrow Flat drift lower edge).

3.3 Deep Drift Profile: High Elevation

We now analyze snow density at a second deep drift location, this time at a higher elevation with a different topographic setting, and we compare our observations to surrounding snow pits that illustrate a variety of interacting controls on density (Fig. 6). Downs Mountain (4071 m elevation) is the northernmost 4000-meter peak on the Rocky Mountain Continental Divide, providing a unique combination of extreme alpine conditions. A 1.6 m snow pit in a drift near the summit (4040 m) has a much lower density of 401 kg/m^3 compared to lower-elevation snow of a similar depth, e.g., 471 kg/m^3 in a 1.1 m snow pit at 3630 m elevation on the nearby Goat Flat plateau (Fig. 1). A 0.8 m snow pit on a steep (43°) north-facing slope also has a relatively low density of 393 kg/m^3 despite being at a similarly low elevation as the relatively dense Goat Flat snow pit (471 kg/m^3). Compared to the nearby summit and north-facing snow pits, 4.0 m deep snow pit in an extensive drifted snowfield at 3820 m elevation has a substantially higher density of 457 kg/m^3, though this is still much less dense than the nivation hollow drifts. Part of this difference in snow density between the deep nivation hollow drift and the deep Downs Mountain snowfield is associated with the latter's 540 m higher elevation, as we show in Sect. 3.4. Finally, a partial snow pit in an avalanche runout zone has the highest average density observed in the Downs Mountain vicinity (483 kg/m^3), and individual blocks of recent wet slide debris have even higher densities in the range of 558-638 kg/m^3.

https://doi.org/10.5194/egusphere-2026-1933
Preprint. Discussion started: 8 May 2026

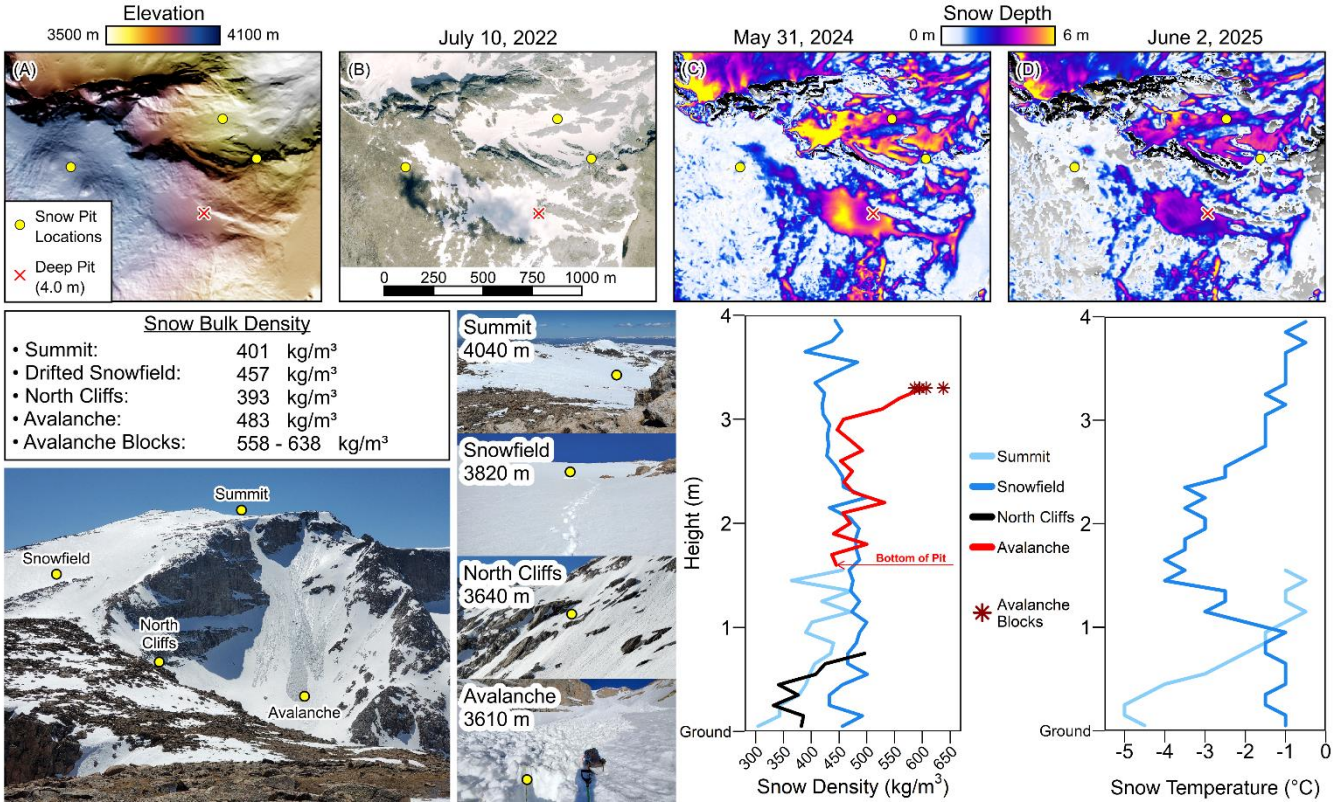

Figure 6. Snow depth maps, density / temperature profiles, and photos of four snow pits in the Downs Mountain environs.

The deeply drifted snowfield on the downwind (east) side of Downs Mountain has a substantially higher density than shallower snow at comparable elevations. The three other snow pits above 3800 m have a mean density of 409 kg/m^3 compared to 457 kg/m^3 in the 4.0 m pit, a difference of about 12%. Considering that one of these three other high-elevation pits is also fairly deep (2.1 m / 438 kg/m^3, near Hunters Hump in the Green River watershed), the drift density is even more pronounced when comparing it only to relatively shallow high-elevation snow (e.g., 387 kg/m^3 for a 0.8 m pit near the upper edge of the Continental Glacier). Conversely, snow density increases rapidly at lower elevations, and even shallow snow is denser than the deep snowfield at altitudes only 200-250 m lower (e.g., 1.1 m / 471 kg/m^3 at 3630 m elevation and 0.8 m / 490 kg/m^3 at 3580 m elevation). Thus, deep wind drifts exhibit consistently higher densities compared to nearby shallower snow, but the absolute magnitude of drift density also depends on elevation and slope/aspect, and hence the snow metamorphosis legacy of the local microclimate.

Despite the onset of ablation at most places in the WRR by the time of our 2025 surveys in late May and early June, some high-elevation snow remained colder than the freezing point, potentially contributing to density variability. Only two of our 36 snow pits show temperatures more than one degree below zero, which is the precision of our analog thermometer. These

https://doi.org/10.5194/egusphere-2026-1933
Preprint. Discussion started: 8 May 2026

two cold locations are the Downs Mountain summit drift (mean -2.4 ˚C, range -0.5 to -5.0 ˚C) and the Downs Mountain deep drifted snowfield (mean -2.0 ˚C, range -0.5 to -4.0 ˚C). Interestingly, the second-highest snow pit (3980 m elevation) shows nearly isothermal temperatures (all temperatures between -1.0 and -0.5 °C), demonstrating that elevation (and air temperature, by proxy) is not the only control on snowpack temperature. Notably, this high-elevation snow pit is half as deep as the Downs Mountain summit drift (0.8 vs. 1.6 m). The coldest temperatures in the Downs Mountain summit drift are near the ground surface, and the snowpack warms to zero near the surface, which suggests that this difference in temperature may be the result of seasonal and/or diurnal insulation effects from the deeper snowpack. Likewise, the deep snowfield reaches a temperature of zero near the surface, though it also warms to zero near the ground, with the coldest snow at a height of 1.4-2.4 m (near the middle of the profile).

Snow temperature had an inconclusive relationship with density at the time of our surveys. There is a weak negative correlation between density and temperature in the deep snowfield ($r = -0.37$, $p = 0.02$), unlike the shallower summit drift, which has a strong positive density-temperature correlation ($r = 0.73$, $p = 0.001$). In the case of the shallower non-isothermal pit, we observe depth hoar (loose facets) near the ground, but the temperature profile is reversed compared to what we would expect for depth hoar formation, which is typically associated with colder surface temperatures and warmer snow near the ground. This temperature reversal could be indicative of the transition between the accumulation and ablation season, as the snowpack ripens and warms from the top down. In contrast, the deep snowfield does not exhibit depth hoar and shows a significant trend toward increased density with depth, which is rare in the WRR at the time of our spring snow surveys (Fig. 3). All of the snow pits in the Downs Mountain vicinity have at least some ice layers, so melt-freeze processes and liquid water percolation probably also contribute to density variations, even though parts of the vertical profile remain below freezing.

3.4 Empirical Snow Density Models

Snow pit measurements at individual locations are useful to inform our understanding of density heterogeneity, but a model is necessary to extrapolate density variations across entire landscapes in order to estimate SWE in combination with lidar-based snow depth maps. In this section, we first evaluate an empirical density model fine-tuned to the 2025 WRR snow pit dataset, which illustrates the relative importance of different factors affecting density. Subsequently, we compare our measurements with several previously reported snow density models from the literature to test whether established models can capture the types of variability observed in the field.

A nonlinear regression model (Eq. 1) can satisfactorily explain density differences between most snow pits in our 2025 dataset. We exclude the two pits from the edges of the nivation hollow since they are not representative of most areas of the snowpack with similar depth. Across the other 34 snow pits, the fitted model has a root-mean-square-error (RMSE) of 26

https://doi.org/10.5194/egusphere-2026-1933
Preprint. Discussion started: 8 May 2026

kg/m^3, which is 6% error relative to the mean of 447 kg/m^3. The coefficient of determination for density variability is R^2 = 0.76 across all 34 of these pits, which increases to R^2 = 0.94 considering only the densities of the eight pits > 2 m deep.

All of the fitted model parameters in Eq. 1 describe relationships that match physical expectations (Fig. 7). The model indicates higher densities at lower elevations, in deeper snow, and in open areas (conversely, density is lower in forested areas). Elevation is a proxy for air temperature, and lower elevations are associated with more melt-freeze cycles and an earlier start to snowpack metamorphosis, leading to higher densities at the time of our surveys. Snow depth is a proxy for accumulation processes such as wind drifting and avalanching, which can increase density by fracturing and sintering grains. Although we do not explicitly investigate processes leading to the observed densities in this study, we expect that forest canopy cover may be associated with lower density snow due to a combination of factors including wind shelter, shade, and nighttime longwave radiation, which could reduce the number of melt-freeze cycles. The model also identifies slightly lower densities on north-facing and east-facing slopes, consistent with fewer melt-freeze cycles caused by overall shading and reduced late-afternoon sun exposure when temperatures are warmest. Since Bayesian sampling (Sect. 2.2.1) inherently quantifies and propagates uncertainty throughout the model fitting procedure, we can robustly estimate confidence intervals for these effect sizes despite our relatively small dataset size. The fitted model is represented by a multivariate posterior distribution (Fig. S3 in the Supplement) instead of discrete parameter values, and the spread of this distribution rigorously quantifies the uncertainty of the model with respect to the interaction of all five variables (Eq. 1). The linear depth-density relationship has an uncertainty of 9% (CV of posterior parameter distribution for θ_2 in Eq. 1), with a 95% confidence interval of 18 to 26 kg/m^3 increase in density per meter increase in depth (vertically integrated between locations, not vertical density variability). The parameter distributions for elevation and canopy cover are less straightforward to interpret since they are multivariate and nonlinear, but 100% of the parameter samples are negative for θ_3 and θ_6, indicating very high confidence that density is lower in the forest and at high elevations. The linear relationships with north and east slope are more weakly constrained due to the limited slope of our observations (max 43°), but the posterior parameter distribution still provides 96% confidence that north-facing slopes have lower densities and 90% confidence that east-facing slopes have lower densities.

https://doi.org/10.5194/egusphere-2026-1933
Preprint. Discussion started: 8 May 2026

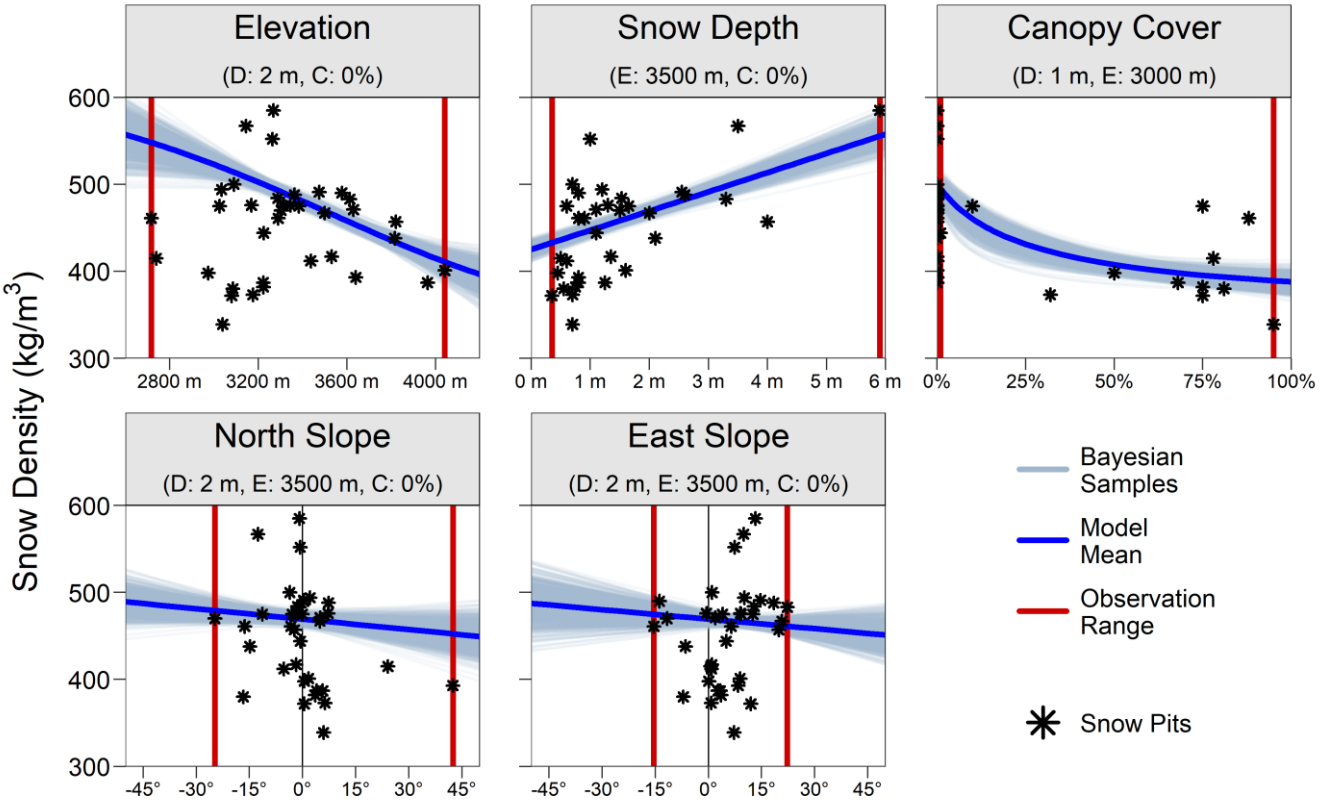

Figure 7. Evaluation of statistical snow density model with respect to individual variables. In each panel, all other variables are held constant, and the snow density response is predicted with respect to a single variable (e.g., for elevation, the snow depth is held constant at 2 m with 0% forest cover). D = snow depth, C = forest cover, E = elevation. All topographic slopes are flat except as specified. Snow pit measurements are shown to illustrate the range of variability, but since each snow pit corresponds to a unique combination of all five predictors, the snow pit points are not expected to fit the univariate sensitivity tests shown here.

Critically, no single predictor dominates the prediction of snow density. Instead, observed snow densities are the result of interactions between multiple factors, e.g., high-elevation deep snow may have the same density as low-elevation shallow snow. This finding is strikingly apparent in Fig. 7: although the directionality and magnitude of the response to each individual predictor is well constrained by the ensemble of Bayesian parameter samples, the observed snow densities vary widely across any single predictor. Together, however, the seven-variable model explains most of the observed spatial variability (r = 0.86), as shown by the scatterplot of modeled and measured snow density in the WRR 2025 panel of Fig. 8. The simpler model from 2024 (no slope/aspect dependence), fitted to multiple years of prior data, also achieves a reasonably high correlation with the 2025 data (r = 0.76) with minimal bias (-2%), suggesting that WRR snow density relationships repeat across years.

https://doi.org/10.5194/egusphere-2026-1933
Preprint. Discussion started: 8 May 2026

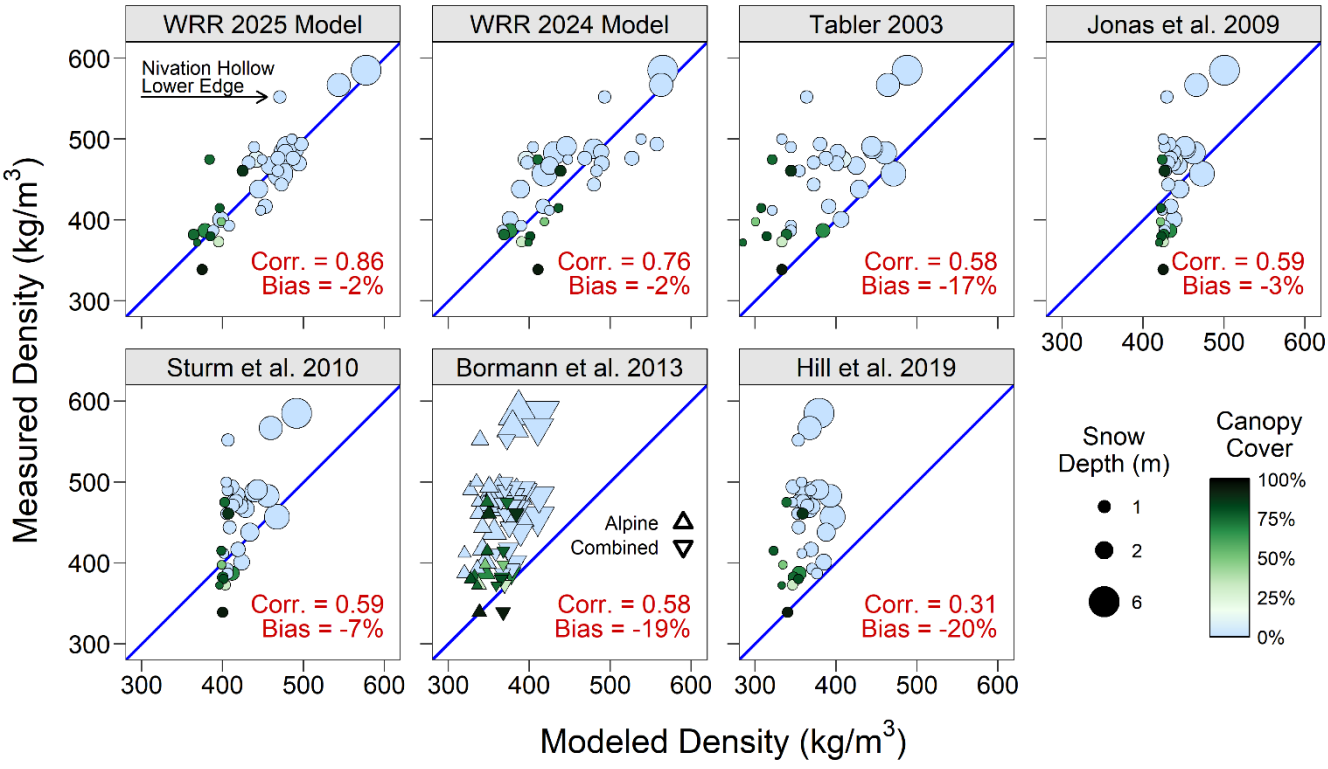

Figure 8. Comparison of measured snow densities with predicted density from various empirical models (Table 1). The WRR 2025 model is directly fit to this dataset, and the WRR 2024 model is fit to various WRR observations from previous years. The other models are based on an array of global observations presented in the literature, and are not necessarily intended for general extrapolation. Correlation and bias for the Bormann et al. (2013) models are reported as averages between the alpine model and the model based on all combined global sites. Note that all of the prior literature models substantially underestimate the highest densities, and most models neglect the density contrast between snow in forested and open areas.

Previous empirical snow density models underestimate the heterogeneity of the WRR snowpack. Each of the panels of Fig. 8 illustrates a different approach to empirical density modeling reported in the literature (Table 1) and evaluated at our snow pit locations. All of these models include at a minimum a regression on snow depth, which itself has a reasonably strong correlation with density across our snow pits ($r = 0.59$, $p < 0.001$), though this relationship is scattered (cf. depth-sensitivity panel of Fig. 7). Since the models proposed by Tabler (2003), Jonas et al. (2009), and Sturm et al. (2010) exclusively use snow depth to infer spatial variability in snow density using various linear and non-linear equations, these models offer little to no additional predictive skill relative to the raw depth-density correlation. By accounting for additional meteorological effects, we would expect the Bormann et al. (2013) multiple linear regression models to account for additional variability. However, since site-specific meteorological data are not available (unlike at the stations where the models were developed), the interpolated gridded meteorological data offer minimal additional predictive skill for snow density. Thus, the Bormann et

https://doi.org/10.5194/egusphere-2026-1933
Preprint. Discussion started: 8 May 2026

al. (2013) models, as adapted for this study, produce similar correlations as the other models (r = 0.57 for the alpine model and r = 0.59 for the combined global site model). The Bormann et al. (2013) global (all-site combo) model has lower bias than the alpine model in the WRR, so we use the global model to evaluate watershed metrics discussed subsequently. The Hill et al. (2019) model also uses gridded climate data (Table 1), but the regression is insufficiently sensitive to snow depth in the WRR, yielding the lowest correlation across all of the tested models (r = 0.31) and largest bias (-20%). The underestimation of density by the Hill et al. (2019) model may partly due to the relatively low December-February estimated precipitation (mean 0.182 m across snow pit locations) compared to the relatively deep measured snow (mean 1.46 m across snow pit locations), since much of the Rocky Mountain snowpack accumulates in spring storms occurring after the December-February "winter precipitation" period (Serreze et al. 2001, Trujillo and Molotch 2014). This low winter precipitation estimate (from gridMET) is roughly congruent with the map presented by Hill et al. (2019) in their Fig. 5B, and the resulting large density bias highlights the risk of relying on gridded climate data aggregated over an arbitrary time period (defined by specific "winter" months) as opposed to the more direct depth-density approach taken by most other models, which can implicitly account for the full accumulation season.

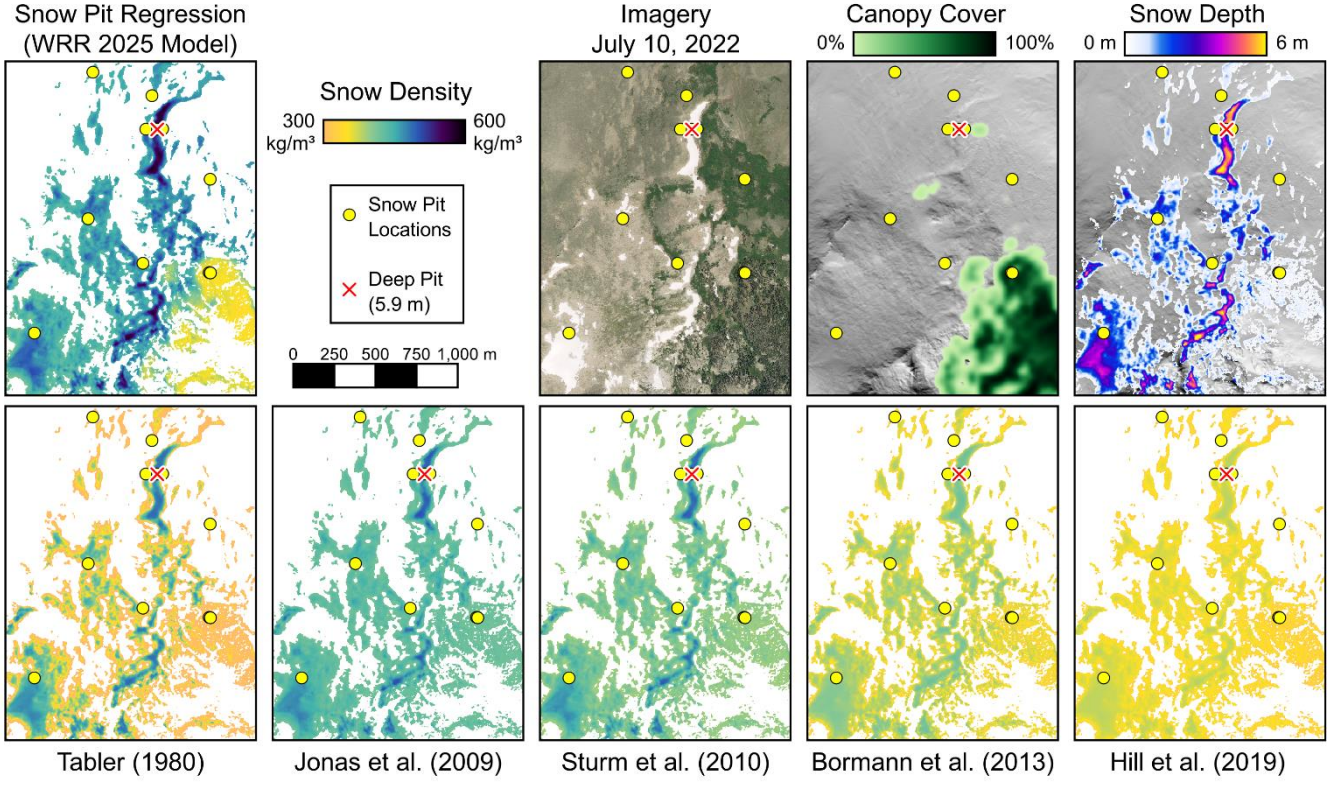

Figure 9. Snow density maps in the region surrounding the Burrow Flat nivation hollow study site (location also shown in Figs. 1, 4, and 5). All of the maps are based on empirical relationships with the lidar-derived snow depth at 3 m resolution in addition to other variables for some models (Table 1); the global combo model is used for Bormann et al. (2013) since it outperformed the alpine model. Note the strong contrast between low-density snow in the forested area and high-density snow in the deep nivation

https://doi.org/10.5194/egusphere-2026-1933
Preprint. Discussion started: 8 May 2026

hollow drift identified by the snow pit regression. Additional snow pits in nearby forest areas (outside map extent) further support this contrast.

None of the prior literature density models considered here numerically parameterize the effect of forest cover, though forest cover is sometimes considered qualitatively (Sturm et al. 1995) when choosing the appropriate climate class for the Sturm et al. (2010) model. Except for the Tabler (2003) model, which has similar bias between forested and open locations, the other models all have significantly more negative biases (greater underestimation of snow density) in non-forested locations, with a statistically significant difference in the bias at the $p < 0.01$ level for all other prior models except Hill et al. (2019), which has a significant bias difference at $p < 0.02$. The explicit consideration of forest cover in Eq. 1 of this study removes this systematic bias, i.e., the difference in forested and non-forested bias for our WRR 2025 and WRR 2024 models is not statistically significant ($p = 0.44$ and 0.45 respectively). The observed density contrast between low-density forest snow and high-density snow in open drifted areas is especially apparent in the Fig. 9 maps. Although the Tabler (2003) indirectly captures this effect because of the confounding effect of snow depth (i.e., forest snow is generally shallower), this model predicts the same low density for shallow snow everywhere, whereas our measurements indicate a systematically higher density in non-forested areas (Figs. 2 and 7).

3.5 Watershed-Scale Snowpack Heterogeneity

Neglecting the high density of alpine wind drifts can lead to substantial underestimation of the total SWE volume in mountain watersheds. Noting again that most of the prior literature snow density models (Fig. 8) are not specifically calibrated to the WRR, applying these models to the 2025 lidar snow depth map can nevertheless inform expectations for the potential sensitivity of SWE to different assumptions about density variability. Indeed, some of these models (e.g., Hill et al. 2019) are explicitly intended to convert depth to SWE at large scales in support of water resource projects. In the three watersheds where our snow pits are located (Torrey Creek, Dinwoody Creek, and upper Green River watersheds; Fig. S1 in the Supplement), the watershed-average snowpack storage on June 1-2, 2025, is 0.18, 0.21, and 0.26 m SWE, respectively, estimated using the lidar depth and the 2025 WRR Bayesian regression model (Eq. 1). Relative to this baseline, the Tabler (2003) model predicts 9-13% less total SWE in these three watersheds, the Jonas et al. (2009) model predicts 3-5% less SWE, the Sturm et al. (2010) model predicts 5-8% less SWE, the Bormann et al. (2013) models predict 16-18% less SWE (all-site model) or 22-24% less SWE (alpine model), and the Hill et al. (2019) model predicts 18-20% less watershed-total SWE.

Metrics related to deep snow storage are particularly sensitive to bulk density assumptions. Previous analysis of the WRR snowpack suggests that the amount of snow deeper than some minimum threshold, e.g., SWE > 2 m, is related to inter-watershed differences in late-summer streamflow and glacier mass loss (Boardman et al. 2025). Our 2025 SWE map based on ASO lidar and the WRR-specific density model (Eq. 1) indicates that 34%, 26%, and 10% of the total snowpack is stored

https://doi.org/10.5194/egusphere-2026-1933
Preprint. Discussion started: 8 May 2026

in areas with SWE > 2 m in the Torrey, Dinwoody, and Green River watersheds, respectively. Relative to this baseline, all of the tested prior literature density models underestimate the watershed-total amount of snow storage in places with > 2 m SWE by 14-57% in Torrey Creek, 14-67% in Dinwoody Creek, and 27-78% in the upper Green River. Even deeper snow (SWE > 4 m) is relevant for constraining certain snow science topics such as snow transport (Boardman 2025). At the time of our surveys, we estimate that areas with SWE > 4 m account for about 6%, 2%, and 0.5% of the total snowpack in the Torrey, Dinwoody, and Green River watersheds, respectively. Analogously, the prior literature snow density models underestimate the amount of snowpack storage in areas with SWE > 4 m by 41-90% in Torrey Creek, 42-88% in Dinwoody Creek, and 34-81% in the upper Green River. However, it is important to note that these percentages are calculated only considering the grid cells with SWE exceeding a discrete threshold in each respective map, so this underestimation is compounded by the shrinking number of grid cells that qualify for inclusion with SWE > 2 m or SWE > 4 m when deep snow density is underestimated (i.e., the SWE is not underestimated by 90% in any single grid cell, but the total volume in areas with SWE strictly exceeding 4 m is underestimated by up to 90%).

Despite the underestimation of deep snow storage by the prior literature density models, all of the lidar-based SWE maps still exhibit much higher spatial heterogeneity compared to the other near-real-time gridded SWE datasets (Fig. 10, Table 2). It is no surprise that the lidar-based SWE maps capture more heterogeneity at the native 3 m resolution, since the other gridded datasets are two orders of magnitude coarser (500+ m) and thus incapable of capturing heterogeneity associated with nivation hollows, cornices, and similar fine-scale snowpack features. However, even after averaging all maps to the same 500 m resolution, the lidar-based SWE map exhibits considerable spatial heterogeneity that is not represented in the SNODAS, U. of Colorado, or U. of Arizona datasets, probably because mountain-scale snow-atmosphere coupling processes are missing from the underlying gridded climate datasets (Mott et al. 2018). Within the combined three-watershed area, the lidar-based SWE map shows an area of 16.8 km^2 with > 1 m of average SWE at 500 m resolution, while the U. of Colorado dataset only shows an analogous area of 0.8 km^2 and the other two datasets have zero area with > 1 m SWE. The standard deviation of 500 m average SWE is 56% higher, 75% higher, and 33% higher in the lidar-based map compared to the SNODAS, U. of Colorado, and U. of Arizona SWE maps, respectively. Remarkably, the SNODAS mean SWE is only 2% lower than the lidar-based mean SWE, but the single deepest grid cell (500 m average) in SNODAS is 61% lower, and SNODAS has 36% more snow-free area, indicating a severe underestimation of spatial heterogeneity within the snow-covered area. Even when further averaging the maps to 1,000 m resolution (Fig. S4 in the Supplement), the lidar-based SWE map has 52% higher standard deviation compared to SNODAS. Aggregated to the same 1,000 m resolution, the lidar-based map shows an area of 8 km^2 with > 1 m SWE compared to zero area with > 1 m SWE in SNODAS despite the near-identical mean SWE in both datasets.

https://doi.org/10.5194/egusphere-2026-1933
Preprint. Discussion started: 8 May 2026

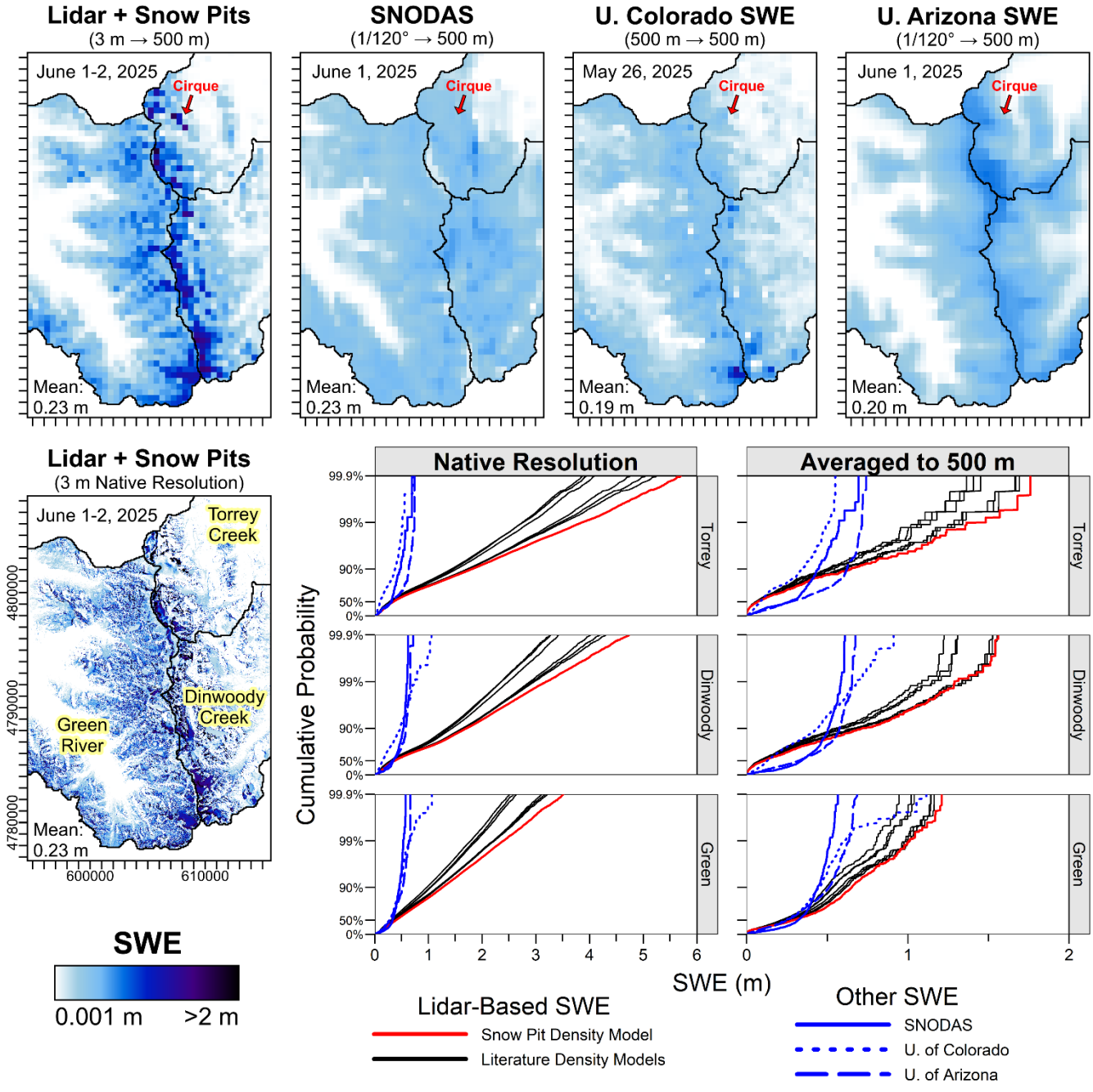

Figure 10. Comparison of gridded SWE datasets in the northern WRR study area. Inset plots show the cumulative distribution function of spatial SWE variability within each map (note logarithmically transformed scale on vertical axis). All datasets are averaged to the same 500 m resolution for consistency (upper panels), though the lidar-based dataset is also shown at the native 3 m resolution for comparison. Regardless of the density model assumptions, the lidar-based SWE map exhibits more spatial heterogeneity than the other datasets, which drastically underestimate the magnitude and spatial extent of deep snow zones. Nevertheless, density model assumptions can also substantially alter the cumulative SWE distribution.

https://doi.org/10.5194/egusphere-2026-1933
Preprint. Discussion started: 8 May 2026

Dataset	Mean SWE (m)	90th, 99th, 99.9th Percentile SWE (m)	Std. Dev. SWE (m)	Area With SWE >1 m (km^2)
Lidar + Snow Pits (3 m)	0.229	0.79, 2.25, 3.82	0.49	55.8
Lidar + Avg. of Five Literature Models (3 m)	0.202	0.70, 1.99, 3.17	0.43	46.8
Lidar + Snow Pits (500 m)	0.230	0.63, 1.17, 1.56	0.28	16.8
SNODAS (at 500 m)	0.226	0.45, 0.56, 0.61	0.18	0
U. Colorado SWE (at 500 m)	0.190	0.43, 0.61, 0.91	0.16	0.8
U. Arizona SWE (at 500 m)	0.201	0.53, 0.66, 0.71	0.21	0

Table 2. Comparison of SWE metrics within the combined Torrey Creek, Dinwoody Creek, and upper Green River watersheds. All five non-WRR literature models from Fig. 9 are averaged for the "Lidar + Avg. of Literature Models" entry. Except for the comparison between the snow pit density model and the literature density models at the native 3 m resolution, all gridded datasets are averaged to 500 m resolution for consistency.

Snow density is an important control on watershed-scale SWE heterogeneity, but all of the lidar-based datasets exhibit more spatial heterogeneity (regardless of which density model is used) in comparison to any of the non-lidar gridded SWE datasets (Table 2). The non-lidar SWE datasets underestimate the watershed-average mean SWE by 2% to 17% compared to an underestimation of 12% on average across all five prior literature density models. At 500 m resolution, the non-lidar gridded SWE datasets underestimate the deepest 90th, 99th, and 99.9th SWE percentiles by a mean of 25%, 48%, and 52%, respectively, while the prior literature density models underestimate the same percentiles by a mean of 11%, 12%, and 17% at 3 m resolution. When considered as a percentage uncertainty, deep snow metrics are relatively more sensitive to snow depth (lidar vs. non-lidar) than snow density (snow pits vs. literature models), and the depth becomes relatively more important compared to density at more extreme SWE percentiles. However, when considering the absolute sensitivity of the SWE distribution, there is a mean difference of 0.09 m SWE between the snow pit and literature-based density assumptions for the 90th SWE percentile compared to a 0.26 m or 0.65 m difference at the 99th and 99.9th percentiles, respectively. Thus, the density constraint has the largest absolute impact on estimated SWE in the deepest parts of the snowpack, as density errors scale multiplicatively with depth.

https://doi.org/10.5194/egusphere-2026-1933
Preprint. Discussion started: 8 May 2026

4 Synthesis and Discussion

4.1 Understanding the Remarkably High Density of Deep Alpine Wind Drifts

In our WRR dataset, the highest bulk snow densities are associated with deep wind drifts at relatively low elevations. Although avalanche debris is the densest snow within the high-elevation Downs Mountain vicinity, even avalanche debris is less dense than the lower-elevation nivation hollow drift, both when considering the mean density of each snow pit (483 vs. 585 kg/m^3) or the highest density of any individual measurement (638 vs. 688 kg/m^3). Unlike glacial firn, which densifies at greater depths (e.g., Stevens et al. 2024), the 5.9 m snow drift density profile exhibits no significant depth-density trend. Since snow near the surface of the drift exceeds the vertically integrated mean density, it seems that overburden pressure is a negligible driver of densification in the nivation hollow drift. This is in contrast to common model parameterizations, such as iSnobal, wherein overburden pressure is the stated driver of densification with depth (Hedrick et al. 2018). Thus, snow lidar surveys relying on modeled density fields may mischaracterize the relationship between depth and density in heavily wind-affected regions such as the WRR. Our finding of constant high density with depth is congruent with expectations for dense packing of snow grains in wind drifts (e.g., Jellinek 1959, Anderson and Benson 1963), though ours appears to be the first literature account of a vertical density profile (at 10 cm resolution) from a 5-6 m drift in an alpine mountain environment. Thus, we are uniquely positioned to test hypotheses about drift density in a mountain environment that is important for western water resources (Bales et al. 2006, Li et al. 2017), as opposed to the Arctic tundra and ice sheet contexts of many older snow drift studies (e.g., Anderson and Benson 1963, Benson and Sturm 1993, Craven and Allison 1998, Sturm et al. 2001, Libois et al. 2014, Parr et al. 2020).

Since our deepest drift profile is very dense even in sections without visible ice layers, and since adjacent snow with a similar microclimate is much less dense, we infer that melt-freeze processes are also unlikely to be the dominant driver of the density contrast between deep and shallow snow. Instead, wind-packing is the obvious explanation for the uniformly high bulk density, which is supported by the distinctive drift morphology (Fig. 4) and wind-topography interactions (Fig. 5). Kotlyakov (1961) found that freshly deposited Antarctic snow can exceed a density of 400 kg/m^3 when deposited during winds of roughly 15-30 m/s (visualized in Fig. III-4 of Mellor 1964), far exceeding the typical density of new snow (Tabler 2003). Consequentially, the correlation between snow depth and density (deeper drifts are generally denser) is not necessarily a causal relationship in windy locations, i.e., depth is not the cause of density variability. Rather, snow depth may function as a proxy for the intensity of wind-driven accumulation processes such as saltation, which is causally linked to wind-packing snow densification (Sommer et al. 2017). In other words, drifting processes increase both the depth and density of certain snowpack locations. Although this finding might be a trivial consequence of spherical geometry from the perspective of grain-scale snow science (Jellinek 1959, Anderson and Benson 1963), Tabler (2003) emphasizes “the pressure of overlying snow” when introducing the relationship between drift depth and density, which would logically lead to greater densities at deeper depths (since there is no overlying snow at the surface), in contrast to our observations. This discrepancy

https://doi.org/10.5194/egusphere-2026-1933
Preprint. Discussion started: 8 May 2026

in the prior snow drift literature indicates that our first-in-class complete density profiles from deep alpine drifts contribute additional evidence in support of wind-packing as the dominant driver of the depth-density correlation in drifted locations. Moreover, grain-scale wind-packing effects on snow density are rarely considered in operational near-real-time SWE quantification (i.e., not considered by iSnobal used for the typical ASO pipeline, Hedricks et al. 2018), and these effects are obviously not captured by in-situ stations located below treeline where major drifts do not occur. For the first time, our study quantifies the watershed-scale impact of ignoring wind-packing effects on snow density.

Wind-packing densification also provides evidence for salient topographic controls on spatial snowpack patterns and the potential repetition of these patterns across years (Pflug and Lundquist 2020). Our computational fluid dynamics modeling of nivation hollow wind speeds in Fig. 5 demonstrates how concave terrain features could plausibly create self-limiting snow drifts, potentially explaining the spatial density variations observed in these locations. The difference in wind speed between the ground and snow surface (Fig. 5C) indicates that as the drift grows, the nivation hollow becomes less effective at reducing near-surface wind speeds, limiting further growth of the drift and producing the nearly identical snow surface profile observed in different years (Fig. 4). This self-limiting behavior could explain why the lower edge of the drift matches the density stratification near the ground in the deep pit: early wind-packed snow covers both areas similarly, but the middle of the nivation hollow continues accumulating snow after the lower edge reaches its equilibrium profile. This behavior could also explain the lower density at the upper edge of the drift, since the top of the drift would only fill with snow after the rest of the drift volume has already accumulated, leaving less time for metamorphosis and densification at the upper edge. Similar drift-trapping behavior in topographic concavities is observed in other alpine environments (e.g., Niwot Ridge, Berg 1986), but our study provides a unique opportunity to visualize this behavior with multiple years of lidar data and computationally verify the underlying wind behavior (Fig. 5). A self-limiting drift-trapping process could also explain why perennial ice patches in similar nivation hollows exhibit very thin annual accumulation layers (Meulendyk et al. 2012, Chellman et al. 2021, Alt et al. 2024). Regardless of the total annual snowfall, a wind-limited equilibrium drift profile could limit net accumulation to match the slow rate of annual compaction, producing the observed thin ice patch accumulation layers. In contrast to the self-limiting nivation hollow location, which exhibits near-identical snow accumulation each year (Fig. 5D-F), the higher elevation drifts in the Downs Mountain vicinity vary widely between years (Fig. 6C-D). The repeat application of lidar surveys across years can thus be used to distinguish filling and non-filling drift zones (Benson and Sturm 1993, Parr et al. 2020).

In contrast to empirical models that generally assume a direct relationship between snow depth and density, including our density model used for this study (Eq. 1), wind-packing densification might be better understood in a discrete spatial context, i.e., within the bounds of the nivation hollow. Instead of viewing snow depth as purely a one-dimensional concept, it may be useful to consider the maximum depth of cohesive drift formations as a proxy for wind-packing intensity. Future density modeling could perhaps leverage a spatial classification of discrete snowpack features to identify where wind-packing may

https://doi.org/10.5194/egusphere-2026-1933
Preprint. Discussion started: 8 May 2026

be important, or process-based simulations could be developed that explicitly simulate the self-limiting drift behavior and associated densification of layered snow facies. Nevertheless, snow depth remains a useful first-order proxy for blowing snow (and hence wind-packing snow density) in our study region, even though the depth-density relationship breaks down at the edges of the nivation hollow (Figs. 4 and 8).

The processes controlling snow drift density are relevant for SWE quantification even at watershed scales. Nivation hollows with drifts as large as the one in Fig. 4-5 are infrequent across the WRR, but snow drifts in general are common in alpine regions. Looking beyond watershed-scale SWE quantification, the nivation hollow drift is also interesting from the perspective of periglacial geomorphology and alpine ecology (Thorn 1976, Wigmore and Molotch 2024), since meltwater from this drift (which persists throughout most of the summer) contributes to accelerated weathering and sustains a downslope wetland (Fig. S5 in the Supplement). In addition to our single exceptionally deep drift profile, our numerous other complete snow pits from the WRR alpine environment constrain drift density across gradients of depth and topography. Neglecting the higher density of deep drifts can lead to systematic underestimation of watershed-scale snowpack storage by as much as 24% (Sect. 3.4). This bias is exacerbated when considering metrics of snowpack heterogeneity, as watershed-total deep snow storage metrics are underestimated by 14-78% (SWE > 2 m) and 34-90% (SWE > 4 m) since the area meeting a respective threshold also decreases when SWE is underestimated in any particular grid cell (e.g., a grid cell underestimated at 3.9 m SWE no longer counts for the SWE > 4 m metric). Although these precise depth thresholds are merely illustrative, deep snowpack metrics in general are important for accurate understanding of snow accumulation processes (Boardman 2025) and snowmelt processes shaping glacier resilience and streamflow seasonality (Boardman et al. 2025), so underestimating the SWE heterogeneity in a watershed could severely hinder these derivative analyses. The lack of any snow pits deeper than 2 m in many prior lidar-based SWE mapping studies (e.g., Broxton et al. 2019, Meehan et al. 2024) limits the utility of these prior datasets for snowpack quantification in alpine mountain regions, where drifts frequently exceed several meters in depth (Fig. 10).

4.2 Missing Snow Density Heterogeneity in Empirical Models

Existing empirical snow density models systematically underestimate the spatial heterogeneity of snow density in the WRR, affecting snowpack analyses at scales ranging from individual snow pits to kilometer-scale watershed metrics (Figs. 8-10). We identify three primary sources of missing heterogeneity: (1) underestimation of snow density in drifted areas affected by wind-packing, (2) failure to quantify systematic differences in snow density between forested and open alpine areas, and (3) missing topographic and microclimatic controls on snow density.

Although each of the prior literature density models (Table 1) considers snow depth as a predictor variable for density, the models tend to underestimate the magnitude of this relationship in the WRR (Fig. 8). Across all 36 snow pits, the literature models have mean biases between -3% and -23%, which is a reasonable level of skill given that these models are based on

https://doi.org/10.5194/egusphere-2026-1933
Preprint. Discussion started: 8 May 2026

mean annual densification rates measured in various locations globally, and the literature models are not necessarily intended for precise snow density prediction at a particular location in a particular year. Nevertheless, it is noteworthy that all five of the literature models systematically underestimate the density of the deep nivation hollow drift (Fig. 4) by -14% to -35%, even the models with minimal bias across all snow pits (Fig. 8). The underlying measurements upon which these models are based do not capture the full range of natural snowpack variability. For example, despite the vast amount of data (11,147 depth-density pairs) used by Jonas et al. (2009), there are no pairs with snow depth > 3.5 m (Fig. 3 of that study). Moreover, deep snow measurements are relatively infrequent in these large model-fitting datasets, leading to models that do not fully capture this heterogeneity (even within the maximum measured range) due to regression dilution and mean centralization. Despite the much smaller size of our dataset (36 snow pits), we structured our survey design to strategically include extreme endmembers, including two complete pits in high- and low-elevation deep drifts of 4-6 m (Fig. 4 and 6). Across the three-watershed region considered here (Fig. 10), 21% of all non-zero lidar snow depth measurements have depth > 2 m, constituting an estimated 56% of the total SWE volume, while 22% of our snow pits are at least 2 m deep, suggesting that deep snow density may still remain under-represented. Prior studies have sometimes only achieved weak or inconclusive empirical models of snow density (e.g., R^2 = 0.29 to 0.39 for modeled vs. measured density, Broxton et al. 2019), which could be partially attributable to sampling a small range of snowpack variability (e.g., snow pit depth range of 0.15 to 1.18 m in that study). Our wide range of sampled snow densities and depths (Fig. 2) manifests in an empirical model describing snow density variations across a relatively large range (R^2 = 0.76 for 34 snow pits or 0.94 for the eight pits > 2 m, Figs. 7-8).

Snow is systematically denser in open areas compared to forested areas (Figs. 2 and 7). This fact, which is trivial to anyone who spends much time walking in the mountains, is nevertheless rarely tested statistically. The forest-open density contrast has been recognized by other studies (Bonner et al. 2022, Meehan et al. 2024), but this distinction remains unaccounted in most large-domain empirical density models (Table 1). Surprisingly, it appears that gridded canopy cover datasets (e.g., RCMAP used here) have not been previously considered as a predictor for empirical snow density models despite the widespread availability of gridded vegetation datasets. Meehan et al. (2024) did consider gridded vegetation metrics derived from lidar (height and distance to vegetation) in their small-domain density extrapolation, but our use of a continental-scale forest cover dataset is more germane to water supply studies across large river basins. For example, gridded canopy cover would naturally fit into the Hill et al. (2019) modeling framework, but it was not considered in their initial list of potential variables (Eq. 6 of that study) despite the consideration of other gridded terrain datasets (e.g., elevation). Perhaps one reason for the historic oversight of gridded vegetation data in prior snow density regressions could be attributed to the overrepresentation of in-situ stations in forested regions, obscuring the forested-open density contrast in the convenience-sampling datasets upon which prior empirical models are often based (e.g., Bormann et al. 2013, Hill et al. 2019). Additionally, in-situ stations are typically located within forest gaps, blurring the distinction between “open” and “forested.”

https://doi.org/10.5194/egusphere-2026-1933
Preprint. Discussion started: 8 May 2026

An important caveat on our inter-model comparisons is that many of the tested models are being pushed beyond their intended scope. For example, we evaluate the Sturm et al. (2010) model using the regression for the alpine climate class based on the map from Sturm et al. (1995), but Sturm et al. (1995) note that mountain snowpacks are a special case that may not fit into any single other climate class because of the high degree of spatial heterogeneity. This caveat from Sturm et al. (1995) seems to present a roadblock to SWE estimation across large mountain domains, since the meteorological data required to choose the appropriate climate classes are not available at high resolutions over entire mountain ranges. However, our nonlinear regression with only five independent variables (Eq. 1) can explain most of the observed variability (Fig. 8), suggesting that the problem of mountain snow heterogeneity is far from unsolvable. Since these snow pit locations are strategically situated to capture likely endmembers of variability, and since similar patterns repeat across our WRR survey datasets from different years (Fig. 8), it appears that our regression approach can successfully explain the majority of density heterogeneity across a mountain region using a parsimonious and physically interpretable set of five variables that are available in any lidar-surveyed region (depth, elevation, forest cover, and north/east slope). Further evaluation of our regression model structure in other mountain ranges with different climates and vegetation could inform to what degree these relationships are generalizable beyond the WRR.

4.3 Missing Snow Density Heterogeneity in the SNOTEL Network

Much of the missing heterogeneity in prior snow density models (Sect. 4.2) appears to stem from the non-representativeness of in-situ monitoring sites where snow density data are routinely collected. In the WRR specifically, all 13 of the currently active (and one other inactive) SNOTEL stations are located below treeline, with a maximum elevation of 3070 m, which is lower than 97% of the SWE volume at the time of our 2025 surveys (Fig. 11). As a result, all but three of the WRR stations were snow-free at the time of our 2025 field surveys. These three stations show inconsistent day-to-day variability indicative of snow bridging and other quality control issues (Goodison et al. 1981), which is exacerbated by the shallow low-elevation snowpack at this time in the season (depth range 0.05-0.51 m). Further, colocation issues between the snow pillow (which measures SWE) and the snow depth sensor (which measures snow depth) could contribute to inconsistent density calculations, especially when the low-elevation snowpack is shallow and patchy. More broadly, all of the 88 active SNOTEL stations in the State of Wyoming are located in forested settings, with adjacent trees visible in each of the station photos. Fig. S3 in the Supplement to Boardman et al. (2025) further illustrates how SNOTEL stations do not capture the range of density variability observed in the WRR in prior years. Empirical density models based on SNOTEL thus lack the data necessary to constrain snow density variations above treeline in the WRR (Fig. 9). This missing heterogeneity highlights the statistical problem with the convenience sampling used by Bormann et al. (2013), Hill et al. (2019), and others, whereby the automatically collected and easily accessible SNOTEL dataset is used for regression modeling without consideration of whether the constituent stations actually constrain the relevant axes of variability (e.g., forested vs. open, high vs. low elevation, deep vs. shallow snow).

https://doi.org/10.5194/egusphere-2026-1933
Preprint. Discussion started: 8 May 2026

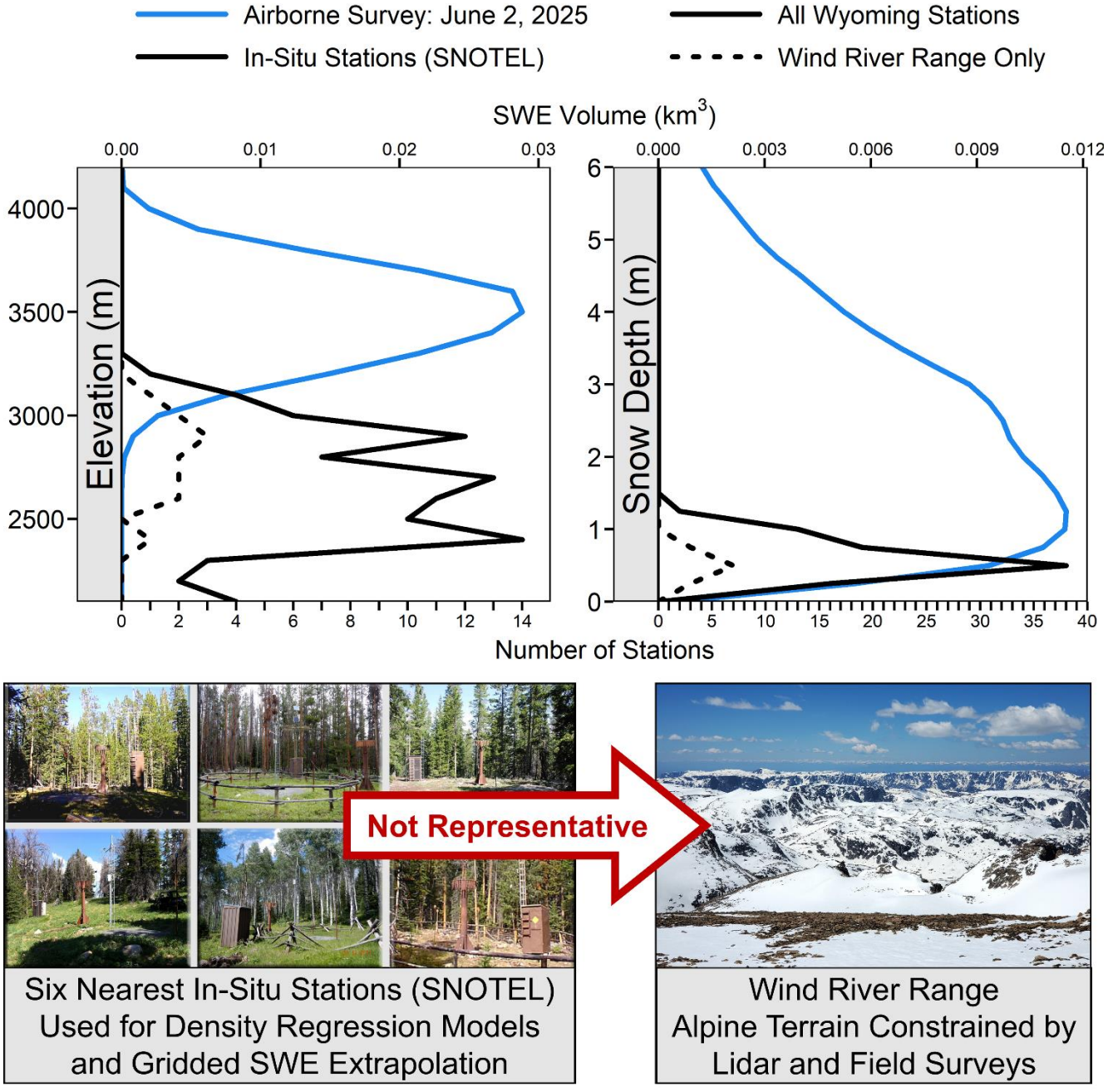

Figure 11: Comparison of elevation and snow depth distribution of the northern WRR snowpack at the time of our June 2, 2025, airborne lidar survey. Note the dual axes on the plots: the top axis shows the volume of SWE (from lidar and snow pit density regression), and the bottom axis shows the number of SNOTEL stations within respective elevation or snow depth bands. The reported SNOTEL snow depth is the maximum depth observed at each site in water year 2025 (most SNOTEL sites were snow-free at the time of our lidar survey). The SNOTEL photos are Natural Resource Conservation Service (NRCS) stock photos (public domain). The alpine photo is from May 31, 2025, looking west into the Green River from Downs Mountain.

https://doi.org/10.5194/egusphere-2026-1933
Preprint. Discussion started: 8 May 2026

Our representativeness score introduced in Sect. 2.2.1 provides robust statistical evidence that our snow pits in deep alpine drifts are more representative than the SNOTEL locations (Fig. 12). The two most-representative snow pits have snow depths around 2.6 m with densities around 490 kg/m^3, more than twice as deep as the deepest ablation-season snow depth (after peak SWE) recorded at any SNOTEL in Wyoming in 2025 (1.16 m). As discussed previous (Sect. 4.1), the absolute deepest drifts are relatively rare across the landscape, but nevertheless the two deepest snow pits (4.0 and 5.9 m) have the third- and fourth-highest representativeness scores. From Fig. 12, it is obvious why extrapolating from the SNOTEL depth-density relationship (or bias-correcting physical models based on SNOTEL data) could lead to unreliable results in the WRR, because the SNOTEL data overlap the least-representative snow pit locations, with anomalously shallow depths and widely scattered densities.

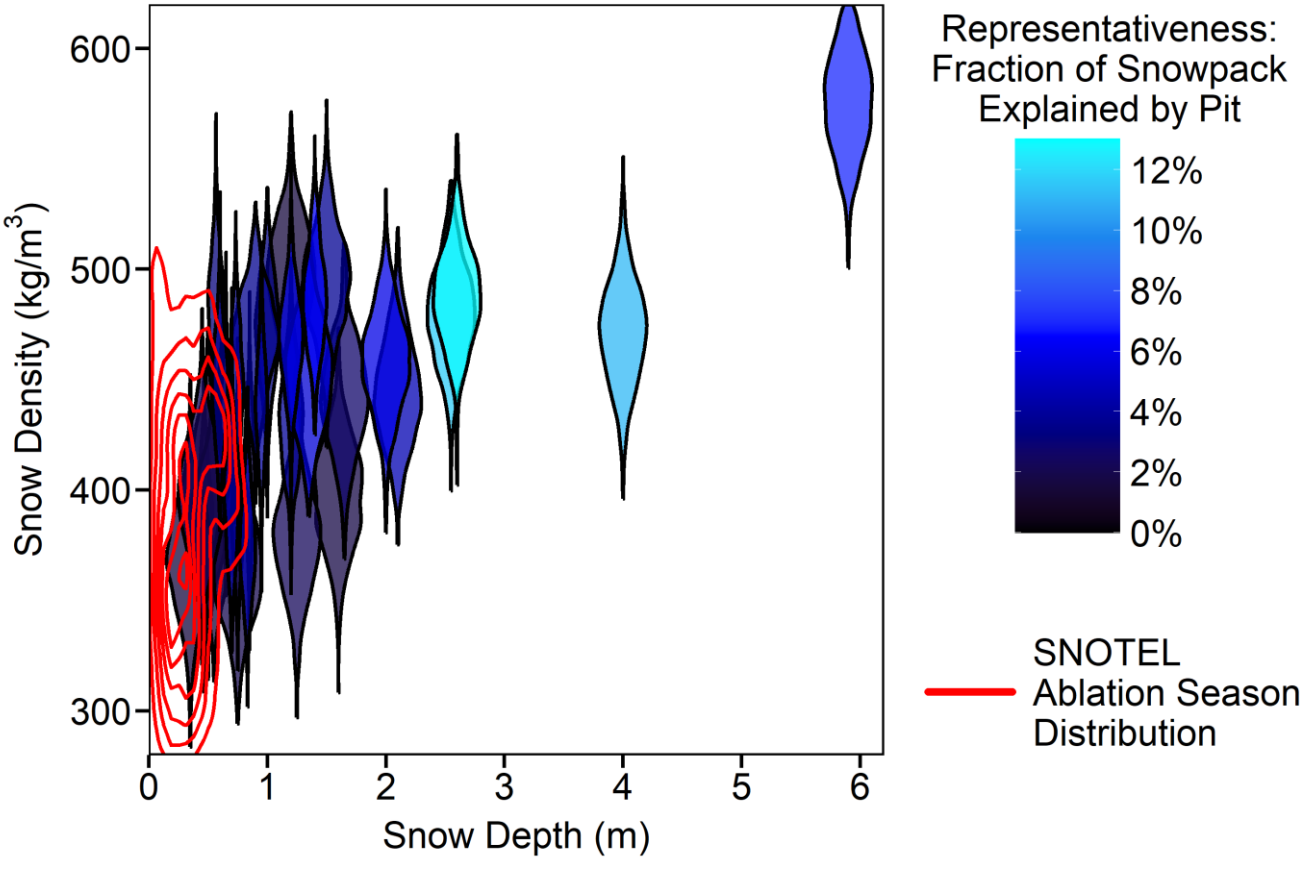

Figure 12: Representativeness of snow pit locations compared to the distribution of SNOTEL data from Wyoming during the 2025 ablation season (beginning from peak SWE at each of 88 SNOTEL locations). Each of the blue violin distributions represents the uncertainty of the Bayesian regression model with respect to a particular snow pit. Lighter blue colors indicate that a particular snow pit is more representative of the WRR lidar-surveyed snowpack as defined in Sect. 2.2.1. The red lines indicate contours of the probability density function (PDF) for the distribution of daily SNOTEL observations of snow depth and density (N = 3676).

https://doi.org/10.5194/egusphere-2026-1933
Preprint. Discussion started: 8 May 2026

Note that the SNOTEL observations are clustered in the least-representative region (shallow snow depth), whereas the most-representative snow pits are between 2 and 4 m deep.

4.4 Missing Heterogeneity in Real-Time Gridded Snowpack Datasets

Boardman (2025) previously argued that kilometer-scale snow transport and redistribution is an underappreciated driver of mountain snowpack patterning, and our analysis here indicates that common spatial snowpack datasets are indeed missing a considerable degree of kilometer-scale heterogeneity (Fig. 10). This missing heterogeneity is likely attributable to extrapolation from non-representative SNOTEL measurements. All three widely available near-real-time gridded SWE datasets analyzed here (SNODAS, U. Colorado SWE, U. Arizona SWE) are based at least in part on the SNOTEL stations discussed previously (Figs. 11-12). The SNODAS product uses a physically based snow model that is "nudged" to better match SNOTEL data, satellite-derived snow-covered area, and potentially other observations when available, though the precise methodology for data selection and assimilation in a particular region or year remains opaque and subject to agency personnel decisions (Barrett 2003). The U. Colorado SWE product (sometimes called SWE-fusion) uses generalized linear regressions to extrapolate spatial SWE from SNOTEL data using physiographic variables, historical SWE patterns (where available), and satellite-derived snow-covered area (Schneider and Molotch 2016, Yang et al. 2022). The U. Arizona SWE product (sometimes called SWANN) uses artificial neural networks to extrapolate spatial SWE from SNOTEL data and other in-situ data using gridded climatology and physiographic variables (Broxton et al. 2016, 2019, 2024). All of these snowpack datasets are available in near-real-time (i.e., within a few days of the nominal date) and are widely used in research across the western USA related to water supply forecasting and other watershed-scale snowpack analyses.

It is unsurprising, yet critically important, that alpine snow drifts and other deep accumulation zones are entirely missing from these gridded datasets in the WRR, because extrapolation from non-representative station data logically leads to a dramatic underestimation of spatial heterogeneity at watershed scales (Figs. 10-11 and Table 2). Researchers considering SNODAS, U. Colorado SWE, or U. Arizona SWE as interchangeable proxies for "spatial SWE datasets" need to understand that these datasets are extrapolated from sparse measurements, which are not necessarily representative of the higher mountain regions where most snow is stored (Fig. 11). Thus, these extrapolated spatial datasets may be useful for estimating a lumped regional snowpack index, but they are unsuitable for studies requiring estimation of actual spatial SWE heterogeneity in the WRR (and potentially in similar alpine regions across the western USA). Our study also underscores the importance of independent validation data for testing common snow data products, which can otherwise become effectively unfalsifiable due to assimilation of all available data (Hedrick et al. 2015).

Gridded SWE products that do not explicitly consider snow transport processes are unlikely to capture the spatial variability of SWE in windy landscapes (Lv et al. 2019). For example, the red arrows in Fig. 10 indicate a particularly notable glacial cirque (43.370°, -109.671°) that collects snow from a roughly 3 km^2 upwind contributing "snowshed" (Boardman 2025). At

https://doi.org/10.5194/egusphere-2026-1933
Preprint. Discussion started: 8 May 2026

500 m resolution, this cirque location is represented by four grid cells with mean SWE of 1.1 to 1.7 m based on our 2025 lidar and snow pit density model. Within the same four 500 m grid cells, the non-lidar gridded datasets show mean SWE of 0.34-0.39 m (SNODAS), 0.25-0.46 m (U. Colorado), and 0.37-0.53 m (U. Arizona). Note that the U. Colorado dataset masks glacier locations, so those values are interpolated from neighboring cells (raw gridded SWE products are shown in Fig. S4 in the Supplement). Comparing the total volume in these four grid cells, the non-lidar SWE datasets underestimate the deep snow storage in this cirque basin by about 65-73% despite much closer agreement with the mean SWE across the whole landscape (e.g., as low as 2% difference for SNODAS, Table 2). Analogously, the five literature density models (Table 1) underestimate the snow storage in the same four grid cells by 9-27%. Accurate measurement of snow depth (from lidar) greatly reduces the uncertainty of deep snow quantification regardless of the density assumption (Fig. 10), but underestimating the density of deep drifts and avalanche debris (Figs. 4 and 6) still causes a substantial underestimation of heterogeneity when applying the prior literature snow density models. Thus, accurate spatial SWE quantification requires accounting for both the extreme depth and extreme density of snow in cirque basins, nivation hollows, and other enhanced accumulation zones affected by both wind transport and avalanches (Fig. 6).

4.5 Transferability

In a scientific era emphasizing “big data” and remote sensing (e.g., Dozier 2011), tedious manual field measurements remain essential. Deep drifts, avalanche runout zones, and steep slopes are globally underrepresented in snow monitoring networks (e.g., Bormann et al. 2013) for obvious practical reasons. Unfortunately, these extreme alpine settings are also typically difficult and/or dangerous to sample manually. To obtain the data in Fig. 6, the lead author assumed personal responsibility (outside the scope of any institutional affiliation) for entering extreme terrain using technical mountaineering gear. These actions were taken after informed acceptance of the associated risks by an individual with extensive personal mountaineering experience in the study region, and obtaining similar measurements could be considered reckless in other circumstances. Moreover, the large amount of manual labor required to sample a very deep drift (Fig. 4) is also prohibitively time-consuming in most circumstances (back-of-the-envelope calculations show that we moved on the order of 10,000 kg of snow just to sample the single deepest 5.9 m snow pit). Our approach also necessitates coordinating the timing of fieldwork with flight planning logistics, which can be challenging in mountain environments with variable weather and multi-day backcountry approach hikes. Thus, comprehensive field surveys of alpine snow density may not always be practical for real-time water supply forecasting applications.

However, even sparse opportunistic measurements from extreme alpine environments can help constrain patterns of snow density that repeat across years (compare WRR 2024-2025 models in Figure 8). These heterogeneous snow density zones are missing from the in-situ station network (Fig. 11) and can advance our understanding of the physical processes underlying variations in snowpack stratigraphy and densification (Figs. 3 and 5). A direct application of our regression model (Eq. 1) to other regions is unlikely to yield the correct mean density due to site-to-site and year-to-year variability, but we anticipate

https://doi.org/10.5194/egusphere-2026-1933
Preprint. Discussion started: 8 May 2026

that our model could nevertheless indicate the degree of potential heterogeneity in other alpine regions associated with deep drifts and forest vs. open areas. We suggest that a greater collaboration between snow scientists and the technical mountaineering community would be useful to further constrain snow heterogeneity in rarely sampled alpine settings globally, but we emphasize that such measurements must be conducted responsibly, perhaps through partnership with professional mountain guides or similar services.

5 Conclusions

Airborne lidar surveys provide the key to accurate quantification of snow depth heterogeneity, which is drastically underestimated by other widely available near-real-time gridded SWE datasets (Fig. 10). However, the availability and quality of alpine snow density information continues to lag the expansion of lidar-based snow depth surveys. In this case, the 2025 ASO WRR lidar survey provides $3x10^7$ non-zero snow depth measurements over the three watersheds considered here, 76% of which are in non-forested areas, but there are only 13 automatic stations providing daily snow density measurements in the WRR, all of which are below treeline with non-representative (shallow) snow depths (Figs. 11-12). More than half of the total surveyed SWE volume is stored in areas with snow depth > 2 m, which is deeper than measured by any in-situ station (Fig. 11). Various physically based and empirical models have been proposed to infer snow density across mountain landscapes, but bias-correcting and validating these models requires representative field data spanning a wide range of environments. The measurements reported here constrain snow density in several rarely sampled settings (e.g., high elevations, avalanche debris, steep slopes, and deep drifts) that can be used to refine empirical parameterizations, motivate the incorporation of missing processes into physically based models (e.g., wind-packing), and inform future field survey plans to efficiently constrain heterogeneity. Spatially explicit SWE estimates must account for the high bulk density and extraordinary depth of alpine wind drifts, which are rarely included in ground-based surveys or monitoring networks and poorly constrained by previous empirical models of both density and SWE (Figs. 8-10). The missing heterogeneity diagnosed here extends from the scale of individual drifts to kilometer grid cells and watershed-scale snowpack statistics (Table 2). Synthesizing lidar surveys with strategic backcountry field measurements can enhance near-real-time spatial SWE quantification, which benefits spatially resolved approaches to water supply forecasting, hydrological and glaciological studies, and other watershed snow assessments.

Code and Data Availability

The data from this study, as well as computer code for data processing and figures, are archived at https://doi.org/10.5281/zenodo.17114675 (Boardman 2025). Lidar data products acquired commercially by Airborne Snow Observatories, Inc. are not included in this archive due to contractual restrictions but are publicly available at https://data.airbornesnowobservatories.com/.

https://doi.org/10.5194/egusphere-2026-1933
Preprint. Discussion started: 8 May 2026

Author Contribution

All authors contributed to data collection during the field surveys and reviewed the manuscript. ENB was the principal investigator for this project, designed the study, and wrote the first draft. AGF contributed to the methodology, validation, and writing. KLB, JAW, JWB, and AAH contributed to visualization and writing (revision). AAH additionally contributed to conceptualization and supervision.

Competing Interests

Author ENB is the owner of Mountain Hydrology LLC, which contracted for data acquisition and partially funded ENB. Author JWB has financial interests in Airborne Snow Observatories, Inc., which acquired the lidar data used here. Authors CAJ, SDS, JAW, and AAH received funding through a Mountain Hydrology LLC subaward to the University of Nevada, Reno.

Acknowledgments

We thank U.S. Forest Service personnel, the Office of the Tribal Water Engineer, and the Wyoming State Engineer's Office for coordinating permissions for WRR snow surveys. Field surveys were conducted within the Fitzpatrick Wilderness of the Shoshone National Forest under Special Use Permit WIN652 issued to Mountain Hydrology LLC. Field surveys were conducted within the Bridger Wilderness of the Bridger-Teton National Forest under Special Use Permit PIN544301 issued to Mountain Hydrology LLC. Field surveys in prior years within the Wind River Indian Reservation were conducted by permission of the Office of the Tribal Water Engineer. We thank Airborne Snow Observatories, Inc., for a large in-kind contribution that supported updating the snow-free lidar data over the WRR glacier surfaces.

Financial Support

Work presented here was funded by U.S. Bureau of Reclamation Award R24AC00025-00.

References

Abatzoglou, J. T.: Development of gridded surface meteorological data for ecological applications and modelling, International Journal of Climatology, 33, 121–131, https://doi.org/10.1002/joc.3413, 2013.

Akitaya, E.: Studies on Depth Hoar, Contributions from the Institute of Low Temperature Science, A26, 1–67, 1974.

Alley, R. B., Bolzan, J. F., and Whillans, I. M.: Polar Firn Densification and Grain Growth, Annals of Glaciology, 3, 7–11, https://doi.org/10.3189/S0260305500002433, 1982.

https://doi.org/10.5194/egusphere-2026-1933
Preprint. Discussion started: 8 May 2026

Alt, M., Puseman, K., Lee, C. M., Pederson, G. T., McConnell, J. R., Chellman, N. J., and McWethy, D. B.: Organic layers preserved in ice patches: A new record of Holocene environmental change on the Beartooth Plateau, USA, The Holocene, 34, 338–352, https://doi.org/10.1177/09596836231211877, 2024.

Anderson, D. L. and Benson, C. S.: The densification and diagenesis of snow, Ice and snow: properties, processes and applications, 391–411, 1963.

Arnaud, L., Lipenkov, V., Barnola, J. M., Gay, M., and Duval, P.: Modelling of the densification of polar firn: characterization of the snow–firn transition, Annals of Glaciology, 26, 39–44, https://doi.org/10.3189/1998AoG26-1-39-44, 1998.

Avanzi, F., De Michele, C., and Ghezzi, A.: On the performances of empirical regressions for the estimation of bulk snow density, Geografia Fisica e Dinamica Quaternaria, 38, 105–112, https://doi.org/10.4461/GFDQ.2015.38.10, 2015.

Bales, R. C., Molotch, N. P., Painter, T. H., Dettinger, M. D., Rice, R., and Dozier, J.: Mountain hydrology of the western United States, Water Resources Research, 42, https://doi.org/10.1029/2005WR004387, 2006.

Barrett, A. P.: National Operational Hydrologic Remote Sensing Center SNOw Data Assimilation System (SNODAS) Products at NSIDC, NSIDC, 2003.

Behrangi, A., Bormann, K. J., and Painter, T. H.: Using the Airborne Snow Observatory to Assess Remotely Sensed Snowfall Products in the California Sierra Nevada, Water Resources Research, 54, 7331–7346, https://doi.org/10.1029/2018WR023108, 2018.

Benson, C. S. and Sturm, M.: Structure and wind transport of seasonal snow on the Arctic slope of Alaska, Annals of Glaciology, 18, 261–267, https://doi.org/10.3189/S0260305500011629, 1993.

Berg, N. H.: A Deterministic Model for Snowdrift Accumulation, in: 1986 International Snow Science Workshop, Lake Tahoe, California, USA, International Snow Science Workshop, 1986.

Boardman, E.: Data and Code for Wind River Range Snow Density Heterogeneity Study, https://doi.org/10.5281/ZENODO.17114675, 2025a.

Boardman, E. N.: Constraining Kilometer-Scale Mountain Snow Transport and Snowshed Areas, Geophysical Research Letters, 52, e2024GL113599, https://doi.org/10.1029/2024GL113599, 2025b.

Boardman, E. N., Fountain, A. G., Boardman, J. W., Painter, T. H., Burgess, E. W., Wilson, L., and Harpold, A. A.: Wind and topography underlie correlation between seasonal snowpack, mountain glaciers, and late-summer streamflow, The Cryosphere, 19, 3193–3225, https://doi.org/10.5194/tc-19-3193-2025, 2025.

Bonner, H. M., Raleigh, M. S., and Small, E. E.: Isolating forest process effects on modelled snowpack density and snow water equivalent, Hydrological Processes, 36, e14475, https://doi.org/10.1002/hyp.14475, 2022.

Bormann, K. J., Westra, S., Evans, J. P., and McCabe, M. F.: Spatial and temporal variability in seasonal snow density, Journal of Hydrology, 484, 63–73, https://doi.org/10.1016/j.jhydrol.2013.01.032, 2013.

https://doi.org/10.5194/egusphere-2026-1933
Preprint. Discussion started: 8 May 2026

Brauchli, T., Trujillo, E., Huwald, H., and Lehning, M.: Influence of Slope-Scale Snowmelt on Catchment Response Simulated With the Alpine3D Model, Water Resources Research, 53, 10723–10739, https://doi.org/10.1002/2017WR021278, 2017.

Broxton, P., Zeng, X., and Dawson, N.: Daily 4 km Gridded SWE and Snow Depth from Assimilated In-Situ and Modeled Data over the Conterminous US, Version 1, https://doi.org/10.5067/0GGPB220EX6A, 2019a.

Broxton, P., Ehsani, M. R., and Behrangi, A.: Improving Mountain Snowpack Estimation Using Machine Learning With Sentinel-1, the Airborne Snow Observatory, and University of Arizona Snowpack Data, Earth and Space Science, 11, e2023EA002964, https://doi.org/10.1029/2023EA002964, 2024.

Broxton, P. D., Dawson, N., and Zeng, X.: Linking snowfall and snow accumulation to generate spatial maps of SWE and snow depth, Earth and Space Science, 3, 246–256, https://doi.org/10.1002/2016EA000174, 2016.

Broxton, P. D., Van Leeuwen, W. J. D., and Biederman, J. A.: Improving Snow Water Equivalent Maps With Machine Learning of Snow Survey and Lidar Measurements, Water Resources Research, 55, 3739–3757, https://doi.org/10.1029/2018WR024146, 2019b.

Brun, E.: Investigation on Wet-Snow Metamorphism in Respect of Liquid-Water Content, Annals of Glaciology, 13, 22–26, https://doi.org/10.3189/S0260305500007576, 1989.

Bühler, Y., Marty, M., Egli, L., Veitinger, J., Jonas, T., Thee, P., and Ginzler, C.: Snow depth mapping in high-alpine catchments using digital photogrammetry, The Cryosphere, 9, 229–243, https://doi.org/10.5194/tc-9-229-2015, 2015.

Chellman, N. J., Pederson, G. T., Lee, C. M., McWethy, D. B., Puseman, K., Stone, J. R., Brown, S. R., and McConnell, J. R.: High elevation ice patch documents Holocene climate variability in the northern Rocky Mountains, Quaternary Science Advances, 3, 100021, https://doi.org/10.1016/j.qsa.2020.100021, 2021.

Colbeck, S. C.: An overview of seasonal snow metamorphism, Reviews of Geophysics, 20, 45–61, https://doi.org/10.1029/RG020i001p00045, 1982.

Colbeck, S. C.: The layered character of snow covers, Reviews of Geophysics, 29, 81–96, https://doi.org/10.1029/90rg02351, 1991.

Craven, M. and Allison, I.: Firnification and the effects of wind-packing on Antarctic snow, Annals of Glaciology, 27, 239–245, https://doi.org/10.3189/1998AoG27-1-239-245, 1998.

Dadic, R., Mott, R., Lehning, M., and Burlando, P.: Wind influence on snow depth distribution and accumulation over glaciers, Journal of Geophysical Research: Earth Surface, 115, https://doi.org/10.1029/2009JF001261, 2010.

Deems, J. S., Painter, T. H., and Finnegan, D. C.: Lidar measurement of snow depth: a review, Journal of Glaciology, 59, 467–479, https://doi.org/10.3189/2013JoG12J154, 2013.

Dohrenwend, J. C.: Nivation Landforms in the Western Great Basin and Their Paleoclimatic Significance, Quat. res., 22, 275–288, https://doi.org/10.1016/0033-5894(84)90022-x, 1984.

Domine, F., Belke-Brea, M., Sarrazin, D., Arnaud, L., Barrere, M., and Poirier, M.: Soil moisture, wind speed and depth hoar formation in the Arctic snowpack, Journal of Glaciology, 64, 990–1002, https://doi.org/10.1017/jog.2018.89, 2018.

https://doi.org/10.5194/egusphere-2026-1933
Preprint. Discussion started: 8 May 2026

Dozier, J.: Mountain hydrology, snow color, and the fourth paradigm, Eos, Transactions, American Geophysical Union, 92, 373–374, https://doi.org/10.1029/2011EO430001, 2011.

Dozier, J., Bair, E. H., and Davis, R. E.: Estimating the spatial distribution of snow water equivalent in the world's mountains, WIREs Water, 3, 461–474, https://doi.org/10.1002/wat2.1140, 2016.

Elder, K., Rosenthal, W., and Davis, R. E.: Estimating the spatial distribution of snow water equivalence in a montane watershed, Hydrol. Process., 12, 1793–1808, https://doi.org/10.1002/(sici)1099-1085(199808/09)12:10/11%253C1793::aid-hyp695%253E3.0.co;2-k, 1998.

Erxleben, J., Elder, K., and Davis, R.: Comparison of spatial interpolation methods for estimating snow distribution in the Colorado Rocky Mountains, Hydrological Processes, 16, 3627–3649, https://doi.org/10.1002/hyp.1239, 2002.

Fierz, C., Armstrong, R. L., Durand, Y., Etchevers, P., Greene, E., McClung, D. M., Nishimura, K., Satyawali, P. K., and Sokratov, S. A.: The International classification for Seasonal Snow on the Ground, UNESCO-IHP, Paris, 2009.

Fleming, S. W., Zukiewicz, L., Strobel, M. L., Hofman, H., and Goodbody, A. G.: SNO^{TEL}, the Soil Climate Analysis Network, and water supply forecasting at the Natural Resources Conservation Service: Past, present, and future, JAWRA Journal of the American Water Resources Association, 59, 585–599, https://doi.org/10.1111/1752-1688.13104, 2023.

Florentine, C., Harper, J., Fagre, D., Moore, J., and Peitzsch, E.: Local topography increasingly influences the mass balance of a retreating cirque glacier, The Cryosphere, 12, 2109–2122, https://doi.org/10.5194/tc-12-2109-2018, 2018.

Freudiger, D., Kohn, I., Seibert, J., Stahl, K., and Weiler, M.: Snow redistribution for the hydrological modeling of alpine catchments, WIREs Water, 4, e1232, https://doi.org/10.1002/wat2.1232, 2017.

Goodison, B. E., Ferguson, H. L., and McKay, G. A.: Measurement and Data Analysis, in: Handbook of Snow: Principles, Processes, Management and Use, edited by: Male, D. H. and Gray, D. M., Blackburn Press, Caldwell, N.J, 191–274, 2004.

Grünewald, T., Stötter, J., Pomeroy, J. W., Dadic, R., Moreno Baños, I., Marturià, J., Spross, M., Hopkinson, C., Burlando, P., and Lehning, M.: Statistical modelling of the snow depth distribution in open alpine terrain, Hydrol. Earth Syst. Sci., 17, 3005–3021, https://doi.org/10.5194/hess-17-3005-2013, 2013.

Hao, J., Mind'je, R., Feng, T., and Li, L.: Performance of snow density measurement systems in snow stratigraphies, Hydrology Research, 52, 834–846, https://doi.org/10.2166/nh.2021.133, 2021.

Harper, J. T. and Bradford, J. H.: Snow stratigraphy over a uniform depositional surface: spatial variability and measurement tools, Cold Regions Science and Technology, 37, 289–298, https://doi.org/10.1016/S0165-232X(03)00071-5, 2003.

Hedrick, A., Marshall, H.-P., Winstral, A., Elder, K., Yueh, S., and Cline, D.: Independent evaluation of the SNODAS snow depth product using regional-scale lidar-derived measurements, The Cryosphere, 9, 13–23, https://doi.org/10.5194/tc-9-13-2015, 2015.

Hedrick, A. R., Marks, D., Havens, S., Robertson, M., Johnson, M., Sandusky, M., Marshall, H.-P., Kormos, P. R., Bormann, K. J., and Painter, T. H.: Direct Insertion of NASA Airborne Snow Observatory-Derived Snow Depth Time

https://doi.org/10.5194/egusphere-2026-1933
Preprint. Discussion started: 8 May 2026

Series Into the iSnobal Energy Balance Snow Model, Water Resources Research, 54, 8045–8063, https://doi.org/10.1029/2018WR023190, 2018.

Henderson, E. P.: Large Nivation Hollows near Knob Lake, Quebec, The Journal of Geology, 64, 607–616, https://doi.org/10.1086/626394, 1956.

Hill, D. F., Burakowski, E. A., Crumley, R. L., Keon, J., Hu, J. M., Arendt, A. A., Wikstrom Jones, K., and Wolken, G. J.: Converting snow depth to snow water equivalent using climatological variables, The Cryosphere, 13, 1767–1784, https://doi.org/10.5194/tc-13-1767-2019, 2019.

Hopkinson, C., Sitar, M., Chasmer, L., and Treitz, P.: Mapping Snowpack Depth beneath Forest Canopies Using Airborne Lidar, Photogrammetric Engineering & Remote Sensing, 70, 323–330, https://doi.org/10.14358/PERS.70.3.323, 2004.

Hörhold, M. W., Kipfstuhl, S., Wilhelms, F., Freitag, J., and Frenzel, A.: The densification of layered polar firn, Journal of Geophysical Research: Earth Surface, 116, https://doi.org/10.1029/2009JF001630, 2011.

Hu, J. M., Shean, D., and Bhushan, S.: Six Consecutive Seasons of High-Resolution Mountain Snow Depth Maps From Satellite Stereo Imagery, Geophysical Research Letters, 50, e2023GL104871, https://doi.org/10.1029/2023GL104871, 2023.

Immerzeel, W. W., Lutz, A. F., Andrade, M., Bahl, A., Biemans, H., Bolch, T., Hyde, S., Brumby, S., Davies, B. J., Elmore, A. C., Emmer, A., Feng, M., Fernández, A., Haritashya, U., Kargel, J. S., Koppes, M., Kraaijenbrink, P. D. A., Kulkarni, A. V., Mayewski, P. A., Nepal, S., Pacheco, P., Painter, T. H., Pellicciotti, F., Rajaram, H., Rupper, S., Sinisalo, A., Shrestha, A. B., Viviroli, D., Wada, Y., Xiao, C., Yao, T., and Baillie, J. E. M.: Importance and vulnerability of the world's water towers, Nature, 577, 364–369, https://doi.org/10.1038/s41586-019-1822-y, 2020.

Jellinek, H. H. G.: Compressive Strength Properties of Snow, Journal of Glaciology, 3, 345–354, https://doi.org/10.3189/S0022143000017019, 1959.

Jonas, T., Marty, C., and Magnusson, J.: Estimating the snow water equivalent from snow depth measurements in the Swiss Alps, Journal of Hydrology, 378, 161–167, https://doi.org/10.1016/j.jhydrol.2009.09.021, 2009.

Judson, A. and Doesken, N.: Density of Freshly Fallen Snow in the Central Rocky Mountains, Bulletin of the American Meteorological Society, 81, 1577–1588, https://doi.org/10.1175/1520-0477(2000)081%253C1577:DOFFSI%253E2.3.CO;2, 2000.

Kanamori, S., Okura, Y., Shiraiwa, T., and Yoshikawa, K.: Snow pit studies and radio-echo soundings on Mt. McKinley 2004, Bulletin of Glaciological Research, 22, 89–97, 2005.

Keenan, E., Wever, N., Dattler, M., Lenaerts, J. T. M., Medley, B., Kuipers Munneke, P., and Reijmer, C.: Physics-based SNOWPACK model improves representation of near-surface Antarctic snow and firn density, The Cryosphere, 15, 1065–1085, https://doi.org/10.5194/tc-15-1065-2021, 2021.

Kinar, N. J. and Pomeroy, J. W.: Measurement of the physical properties of the snowpack, Reviews of Geophysics, 53, 481–544, https://doi.org/10.1002/2015RG000481, 2015.

https://doi.org/10.5194/egusphere-2026-1933
Preprint. Discussion started: 8 May 2026

Kirchner, P. B., Bales, R. C., Molotch, N. P., Flanagan, J., and Guo, Q.: LiDAR measurement of seasonal snow accumulation along an elevation gradient in the southern Sierra Nevada, California, Hydrology and Earth System Sciences, 18, 4261–4275, https://doi.org/10.5194/hess-18-4261-2014, 2014.

Kotlyakov, V. M.: Antarctic Snow Cover and its Role in the Present-day the Glaciations of the Continent, USSR Academy of Science, Moscow, 246 pp., 1961.

Li, D., Wrzesien, M. L., Durand, M., Adam, J., and Lettenmaier, D. P.: How much runoff originates as snow in the western United States, and how will that change in the future?, Geophysical Research Letters, 44, 6163–6172, https://doi.org/10.1002/2017GL073551, 2017.

Libois, Q., Picard, G., Arnaud, L., Morin, S., and Brun, E.: Modeling the impact of snow drift on the decameter-scale variability of snow properties on the Antarctic Plateau, Journal of Geophysical Research: Atmospheres, 119, 11,662-11,681, https://doi.org/10.1002/2014JD022361, 2014.

López-Moreno, J. I., Fassnacht, S. R., Heath, J. T., Musselman, K. N., Revuelto, J., Latron, J., Morán-Tejeda, E., and Jonas, T.: Small scale spatial variability of snow density and depth over complex alpine terrain: Implications for estimating snow water equivalent, Advances in Water Resources, 55, 40–52, https://doi.org/10.1016/j.advwatres.2012.08.010, 2013.

Luce, C. H., Tarboton, D. G., and Cooley, K. R.: The influence of the spatial distribution of snow on basin-averaged snowmelt, Hydrol. Process., 12, 1671–1683, https://doi.org/10.1002/(SICI)1099-1085(199808/09)12:10/11%253C1671::AID-HYP688%253E3.0.CO;2-N, 1998.

Lundquist, J. D., Dettinger, M. D., and Cayan, D. R.: Snow-fed streamflow timing at different basin scales: Case study of the Tuolumne River above Hetch Hetchy, Yosemite, California, Water Resources Research, 41, https://doi.org/10.1029/2004WR003933, 2005.

Lv, Z., Pomeroy, J. W., and Fang, X.: Evaluation of SNODAS Snow Water Equivalent in Western Canada and Assimilation Into a Cold Region Hydrological Model, Water Resources Research, 55, 11166–11187, https://doi.org/10.1029/2019WR025333, 2019.

Mankin, J. S., Viviroli, D., Singh, D., Hoekstra, A. Y., and Diffenbaugh, N. S.: The potential for snow to supply human water demand in the present and future, Environ. Res. Lett., 10, 114016, https://doi.org/10.1088/1748-9326/10/11/114016, 2015.

Marsh, C. B., Lv, Z., Vionnet, V., Harder, P., Spiteri, R. J., and Pomeroy, J. W.: Snowdrift-Permitting Simulations of Seasonal Snowpack Processes Over Large Mountain Extents, Water Resources Research, 60, e2023WR036948, https://doi.org/10.1029/2023WR036948, 2024.

Marsh, P. and Woo, M.: Wetting front advance and freezing of meltwater within a snow cover: 1. Observations in the Canadian Arctic, Water Resources Research, 20, 1853–1864, https://doi.org/10.1029/WR020i012p01853, 1984.

Marshall, H. P., Conway, H., and Rasmussen, L. A.: Snow densification during rain, Cold Regions Science and Technology, 30, 35–41, https://doi.org/10.1016/S0165-232X(99)00011-7, 1999.

https://doi.org/10.5194/egusphere-2026-1933
Preprint. Discussion started: 8 May 2026

Medley, B., Joughin, I., Das, S. B., Steig, E. J., Conway, H., Gogineni, S., Criscitiello, A. S., McConnell, J. R., Smith, B. E., van den Broeke, M. R., Lenaerts, J. T. M., Bromwich, D. H., and Nicolas, J. P.: Airborne-radar and ice-core observations of annual snow accumulation over Thwaites Glacier, West Antarctica confirm the spatiotemporal variability of global and regional atmospheric models, Geophysical Research Letters, 40, 3649–3654, https://doi.org/10.1002/grl.50706, 2013.

Meehan, T. G., Hojatimalekshah, A., Marshall, H.-P., Deeb, E. J., O'Neel, S., McGrath, D., Webb, R. W., Bonnell, R., Raleigh, M. S., Hiemstra, C., and Elder, K.: Spatially distributed snow depth, bulk density, and snow water equivalent from ground-based and airborne sensor integration at Grand Mesa, Colorado, USA, The Cryosphere, 18, 3253–3276, https://doi.org/10.5194/tc-18-3253-2024, 2024.

Mellor, M.: Properties of snow, 1964.

Meulendyk, T., Moorman, B. J., Andrews, T. D., and MacKAY, G.: Morphology and Development of Ice Patches in Northwest Territories, Canada, Arctic, 65, 43–58, 2012.

Molotch, N. P. and Bales, R. C.: SNOTEL representativeness in the Rio Grande headwaters on the basis of physiographics and remotely sensed snow cover persistence, Hydrological Processes, 20, 723–739, https://doi.org/10.1002/hyp.6128, 2006.

Mortimer, C., Mudryk, L., Cho, E., Derksen, C., Brady, M., and Vuyovich, C.: Use of multiple reference data sources to cross-validate gridded snow water equivalent products over North America, The Cryosphere, 18, 5619–5639, https://doi.org/10.5194/tc-18-5619-2024, 2024.

Mott, R. and Lehning, M.: Meteorological Modeling of Very High-Resolution Wind Fields and Snow Deposition for Mountains, Journal of Hydrometeorology, 11, 934–949, https://doi.org/10.1175/2010JHM1216.1, 2010.

Mott, R., Schirmer, M., Bavay, M., Grünewald, T., and Lehning, M.: Understanding snow-transport processes shaping the mountain snow-cover, The Cryosphere, 4, 545–559, https://doi.org/10.5194/tc-4-545-2010, 2010.

Mott, R., Vionnet, V., and Grünewald, T.: The Seasonal Snow Cover Dynamics: Review on Wind-Driven Coupling Processes, Front. Earth Sci., 6, https://doi.org/10.3389/feart.2018.00197, 2018.

Mott, R., Wolf, A., Kehl, M., Kunstmann, H., Warscher, M., and Grünewald, T.: Avalanches and micrometeorology driving mass and energy balance of the lowest perennial ice field of the Alps: a case study, The Cryosphere, 13, 1247–1265, https://doi.org/10.5194/tc-13-1247-2019, 2019.

Musselman, K. N., Pomeroy, J. W., Essery, R. L. H., and Leroux, N.: Impact of windflow calculations on simulations of alpine snow accumulation, redistribution and ablation, Hydrological Processes, 29, 3983–3999, https://doi.org/10.1002/hyp.10595, 2015.

Nolan, M., Larsen, C., and Sturm, M.: Mapping snow depth from manned aircraft on landscape scales at centimeter resolution using structure-from-motion photogrammetry, The Cryosphere, 9, 1445–1463, https://doi.org/10.5194/tc-9-1445-2015, 2015.

https://doi.org/10.5194/egusphere-2026-1933
Preprint. Discussion started: 8 May 2026

Pagano, T., Garen, D., and Sorooshian, S.: Evaluation of Official Western U.S. Seasonal Water Supply Outlooks, 1922–2002, Journal of Hydrometeorology, 5, 896–909, https://doi.org/10.1175/1525-7541(2004)005%253C0896:EOOWUS%253E2.0.CO;2, 2004.

Painter, T. H., Berisford, D. F., Boardman, J. W., Bormann, K. J., Deems, J. S., Gehrke, F., Hedrick, A., Joyce, M., Laidlaw, R., Marks, D., Mattmann, C., McGurk, B., Ramirez, P., Richardson, M., Skiles, S. M., Seidel, F. C., and Winstral, A.: The Airborne Snow Observatory: Fusion of scanning lidar, imaging spectrometer, and physically-based modeling for mapping snow water equivalent and snow albedo, Remote Sensing of Environment, 184, 139–152, https://doi.org/10.1016/j.rse.2016.06.018, 2016.

Parr, C., Sturm, M., and Larsen, C.: Snowdrift Landscape Patterns: An Arctic Investigation, Water Resources Research, 56, e2020WR027823, https://doi.org/10.1029/2020WR027823, 2020.

Pflug, J. M. and Lundquist, J. D.: Inferring Distributed Snow Depth by Leveraging Snow Pattern Repeatability: Investigation Using 47 Lidar Observations in the Tuolumne Watershed, Sierra Nevada, California, Water Resources Research, 56, e2020WR027243, https://doi.org/10.1029/2020WR027243, 2020.

Pomeroy, J. W., Gray, D. M., Shook, K. R., Toth, B., Essery, R. L. H., Pietroniro, A., and Hedstrom, N.: An evaluation of snow accumulation and ablation processes for land surface modelling, Hydrol. Process., 12, 2339–2367, https://doi.org/10.1002/(sici)1099-1085(199812)12:15%253C2339::aid-hyp800%253E3.0.co;2-l, 1998.

Proksch, M., Rutter, N., Fierz, C., and Schneebeli, M.: Intercomparison of snow density measurements: bias, precision, and vertical resolution, The Cryosphere, 10, 371–384, https://doi.org/10.5194/tc-10-371-2016, 2016.

Raderschall, N., Lehning, M., and Schär, C.: Fine-scale modeling of the boundary layer wind field over steep topography, Water Resources Research, 44, https://doi.org/10.1029/2007WR006544, 2008.

Raleigh, M. S. and Small, E. E.: Snowpack density modeling is the primary source of uncertainty when mapping basin-wide SWE with lidar, Geophysical Research Letters, 44, 3700–3709, https://doi.org/10.1002/2016GL071999, 2017.

Raleigh, M. S., Lundquist, J. D., and Clark, M. P.: Exploring the impact of forcing error characteristics on physically based snow simulations within a global sensitivity analysis framework, Hydrology and Earth System Sciences, 19, 3153–3179, https://doi.org/10.5194/hess-19-3153-2015, 2015.

Rigge, M. B., Bunde, B., Shi, H., and Postma, K.: Rangeland Condition Monitoring Assessment and Projection (RCMAP) Fractional Component Time-Series Across the Western U.S. 1985-2020 (2.0, October 2021), https://doi.org/10.5066/P95IQ4BT, 2021.

Roebber, P. J., Bruening, S. L., Schultz, D. M., and Cortinas, J. V.: Improving Snowfall Forecasting by Diagnosing Snow Density, Weather and Forecasting, 18, 264–287, https://doi.org/10.1175/1520-0434(2003)018%253C0264:ISFBDS%253E2.0.CO;2, 2003.

Rutter, N., Essery, R., Pomeroy, J., Altimir, N., Andreadis, K., Baker, I., Barr, A., Bartlett, P., Boone, A., Deng, H., Douville, H., Dutra, E., Elder, K., Ellis, C., Feng, X., Gelfan, A., Goodbody, A., Gusev, Y., Gustafsson, D., Hellström, R., Hirabayashi, Y., Hirota, T., Jonas, T., Koren, V., Kuragina, A., Lettenmaier, D., Li, W.-P., Luce, C., Martin, E.,

https://doi.org/10.5194/egusphere-2026-1933
Preprint. Discussion started: 8 May 2026

Nasonova, O., Pumpanen, J., Pyles, R. D., Samuelsson, P., Sandells, M., Schädler, G., Shmakin, A., Smirnova, T. G., Ståhli, M., Stöckli, R., Strasser, U., Su, H., Suzuki, K., Takata, K., Tanaka, K., Thompson, E., Vesala, T., Viterbo, P., Wiltshire, A., Xia, K., Xue, Y., and Yamazaki, T.: Evaluation of forest snow processes models (SnowMIP2), Journal of Geophysical Research: Atmospheres, 114, https://doi.org/10.1029/2008JD011063, 2009.

Rutter, N., Sandells, M. J., Derksen, C., King, J., Toose, P., Wake, L., Watts, T., Essery, R., Roy, A., Royer, A., Marsh, P., Larsen, C., and Sturm, M.: Effect of snow microstructure variability on Ku-band radar snow water equivalent retrievals, The Cryosphere, 13, 3045–3059, https://doi.org/10.5194/tc-13-3045-2019, 2019.

Safa, H., Krogh, S. A., Greenberg, J., Kostadinov, T. S., and Harpold, A. A.: Unraveling the Controls on Snow Disappearance in Montane Conifer Forests Using Multi-Site Lidar, Water Resources Research, 57, e2020WR027522, https://doi.org/10.1029/2020WR027522, 2021.

Schaerer, P.: The Yield of Avalanche Snow at Rogers Pass, British Columbia, Canada, Journal of Glaciology, 34, 188–193, https://doi.org/10.3189/S0022143000032226, 1988.

Schneider, D. and Molotch, N. P.: Real-time estimation of snow water equivalent in the Upper Colorado River Basin using MODIS-based SWE Reconstructions and SNOTEL data, Water Resources Research, 52, 7892–7910, https://doi.org/10.1002/2016WR019067, 2016.

Schneider, D., Molotch, N. P., Deems, J. S., and Painter, T. H.: Analysis of topographic controls on depletion curves derived from airborne lidar snow depth data, Hydrology Research, 52, 253–265, https://doi.org/10.2166/nh.2020.267, 2020.

Seligman, G.: Snow Structure and Ski Fields: being an Account of Snow and Ice Forms met with in Nature and a study on Avalanches and Snowcraft, Macmillan and Co., Ltd., London, 555 pp., 1936.

Serreze, M. C., Clark, M. P., and Frei, A.: Characteristics of large snowfall events in the montane western United States as examined using snowpack telemetry (SNOTEL) data, Water Resources Research, 37, 675–688, https://doi.org/10.1029/2000WR900307, 2001.

Sommer, C. G., Lehning, M., and Fierz, C.: Wind tunnel experiments: saltation is necessary for wind-packing, Journal of Glaciology, 63, 950–958, https://doi.org/10.1017/jog.2017.53, 2017.

Sommerfeld, R. A. and LaChapelle, E.: The Classification of Snow Metamorphism, Journal of Glaciology, 9, 3–18, https://doi.org/10.3189/S0022143000026757, 1970.

Stevens, C. M., Sass, L., Florentine, C., McNeil, C., Baker, E., and Bollen, K.: Direct measurements of firn-density evolution from 2016 to 2022 at Wolverine Glacier, Alaska, Journal of Glaciology, 1–11, https://doi.org/10.1017/jog.2024.24, 2024.

Sturm, M. and Benson, C. S.: Vapor transport, grain growth and depth-hoar development in the subarctic snow, Journal of Glaciology, 43, 42–59, https://doi.org/10.3189/S0022143000002793, 1997.

Sturm, M., Holmgren, J., and Liston, G. E.: A Seasonal Snow Cover Classification System for Local to Global Applications, Journal of Climate, 8, 1261–1283, https://doi.org/10.1175/1520-0442(1995)008%253C1261:ASSCCS%253E2.0.CO;2, 1995.

https://doi.org/10.5194/egusphere-2026-1933
Preprint. Discussion started: 8 May 2026

Sturm, M., Liston ,Glen E., Benson ,Carl S., and and Holmgren, J.: Characteristics and Growth of a Snowdrift in Arctic Alaska, U.S.A., Arctic, Antarctic, and Alpine Research, 33, 319–329, https://doi.org/10.1080/15230430.2001.12003436, 2001.

Sturm, M., Taras, B., Liston, G. E., Derksen, C., Jonas, T., and Lea, J.: Estimating Snow Water Equivalent Using Snow Depth Data and Climate Classes, Journal of Hydrometeorology, 11, 1380–1394, https://doi.org/10.1175/2010JHM1202.1, 2010.

Sun, L., Zhang, X., Wang, H., Xiao, P., and Wang, Y.: Estimating Daily Snow Density Through a Spatiotemporal Random Forest Model, Water Resources Research, 60, e2023WR036942, https://doi.org/10.1029/2023WR036942, 2024.

Tabler, R. D.: Geometry and Density of Drifts Formed by Snow Fences, Journal of Glaciology, 26, 405–419, https://doi.org/10.3189/S0022143000010935, 1980.

Tabler, R. D.: Controlling Blowing and Drifting Snow with Snow Fences and Road Design, National Cooperative Highway Research Program Transportation Research Board of the National Academies, Niwot CO, 2003.

Thorn, C. E.: Quantitative evaluation of nivation in the Colorado Front Range, GSA Bulletin, 87, 1169–1178, https://doi.org/10.1130/0016-7606(1976)87%253C1169:QEONIT%253E2.0.CO;2, 1976.

Trujillo, E. and Molotch, N. P.: Snowpack regimes of the Western United States, Water Resources Research, 50, 5611–5623, https://doi.org/10.1002/2013WR014753, 2014.

Trujillo, E., Hedrick, A., and Marks, D.: Spatial and temporal features of snow water equivalent across a headwater catchment in the Sierra Nevada, USA, EGUsphere, 1–37, https://doi.org/10.5194/egusphere-2025-3736, 2025.

Tsang, L., Durand, M., Derksen, C., Barros, A. P., Kang, D.-H., Lievens, H., Marshall, H.-P., Zhu, J., Johnson, J., King, J., Lemmetyinen, J., Sandells, M., Rutter, N., Siqueira, P., Nolin, A., Osmanoglu, B., Vuyovich, C., Kim, E., Taylor, D., Merkouriadi, I., Brucker, L., Navari, M., Dumont, M., Kelly, R., Kim, R. S., Liao, T.-H., Borah, F., and Xu, X.: Review article: Global monitoring of snow water equivalent using high-frequency radar remote sensing, The Cryosphere, 16, 3531–3573, https://doi.org/10.5194/tc-16-3531-2022, 2022.

Varhola, A., Coops, N. C., Weiler, M., and Moore, R. D.: Forest canopy effects on snow accumulation and ablation: An integrative review of empirical results, Journal of Hydrology, 392, 219–233, https://doi.org/10.1016/j.jhydrol.2010.08.009, 2010.

Venäläinen, P., Luojus, K., Lemmetyinen, J., Pulliainen, J., Moisander, M., and Takala, M.: Impact of dynamic snow density on GlobSnow snow water equivalent retrieval accuracy, The Cryosphere, 15, 2969–2981, https://doi.org/10.5194/tc-15-2969-2021, 2021.

Wagenbrenner, N. S., Forthofer, J. M., Page, W. G., and Butler, B. W.: Development and Evaluation of a Reynolds-Averaged Navier–Stokes Solver in WindNinja for Operational Wildland Fire Applications, Atmosphere, 10, 672, https://doi.org/10.3390/atmos10110672, 2019.

Weller, H. G., Tabor, G., Jasak, H., and Fureby, C.: A tensorial approach to computational continuum mechanics using object-oriented techniques, Computers in Physics, 12, 620–631, https://doi.org/10.1063/1.168744, 1998.

https://doi.org/10.5194/egusphere-2026-1933
Preprint. Discussion started: 8 May 2026

Wetlaufer, K., Hendrikx, J., and Marshall, L.: Spatial Heterogeneity of Snow Density and Its Influence on Snow Water Equivalence Estimates in a Large Mountainous Basin, Hydrology, 3, 3, https://doi.org/10.3390/hydrology3010003, 2016.

Wigmore, O. and Molotch, N. P.: Snow drifts as a driver of alpine plant productivity as observed from weekly multispectral drone imagery, Ecohydrology, 17, e2694, https://doi.org/10.1002/eco.2694, 2024.

Wirz, V., Schirmer, M., Gruber, S., and Lehning, M.: Spatio-temporal measurements and analysis of snow depth in a rock face, The Cryosphere, 5, 893–905, https://doi.org/10.5194/tc-5-893-2011, 2011.

Yang, K., Musselman, K. N., Rittger, K., Margulis, S. A., Painter, T. H., and Molotch, N. P.: Combining ground-based and remotely sensed snow data in a linear regression model for real-time estimation of snow water equivalent, Advances in Water Resources, 160, 104075, https://doi.org/10.1016/j.advwatres.2021.104075, 2022.

Yang, K., Rittger, K., Musselman, K. N., Bair, E. H., Dozier, J., Margulis, S. A., Painter, T. H., and Molotch, N. P.: Intercomparison of snow water equivalent products in the Sierra Nevada California using airborne snow observatory data and ground observations, Front. Earth Sci., 11, https://doi.org/10.3389/feart.2023.1106621, 2023.

Zemp, M., Hoelzle, M., and Haeberli, W.: Six decades of glacier mass-balance observations: a review of the worldwide monitoring network, Annals of Glaciology, 50, 101–111, https://doi.org/10.3189/172756409787769591, 2009.